

1

2 **Topography of corticopontine projections is controlled by postmitotic**  
3 **expression of the area-mapping gene Nr2f1**

4

5 Chiara Tocco<sup>1\*</sup>, Martin Øvsthus<sup>2\*</sup>, Jan G. Bjaalie<sup>2</sup>, Trygve B. Leergaard<sup>2#</sup>, Michèle Studer<sup>1#</sup>

6

7 <sup>1</sup>*Université Côte d'Azur, CNRS, Inserm, iBV, France*

8 <sup>2</sup>*Institute of Basic Medical Sciences, University of Oslo, Oslo, Norway*

9

10 \*These authors have contributed equally to the study.

11 #Co-last authors.

12 @Corresponding author:

13 Michèle Studer

14 iBV - Institut de Biologie Valrose

15 Univ. Côte d'Azur

16 Centre de Biochimie ; UFR Sciences

17 Parc Valrose, 28 avenue Valrose

18 06108 Nice Cedex 2

19 France

20 Tel.: +33 489150720

21 e-mail: Michele.studer@unice.fr

22

23 **SUMMARY**

24 Axonal projections from layer V neurons of distinct neocortical areas are topographically  
25 organized into discrete clusters within the pontine nuclei during the establishment of  
26 voluntary movements. However, the molecular determinants controlling corticopontine  
27 connectivity are insufficiently understood. Here, we show that an intrinsic cortical genetic  
28 program driven by *Nr2f1* graded expression in cortical progenitors and postmitotic neurons is  
29 directly implicated in the organization of corticopontine topographic mapping. Transgenic  
30 mice lacking cortical expression of *Nr2f1* and exhibiting areal organization defects were used  
31 as model systems to investigate the arrangement of corticopontine projections. Combining  
32 three-dimensional digital brain atlas tools, *Cre*-dependent mouse lines, and axonal tracing,  
33 we show that *Nr2f1* expression in postmitotic neurons spatially and temporally controls  
34 somatosensory topographic projections, whereas expression in progenitor cells influences  
35 the ratio between corticopontine and corticospinal fibers passing the pontine nuclei. We  
36 conclude that cortical gradients of area patterning genes are directly implicated in the  
37 establishment of a topographic somatotopic mapping from the cortex onto pontine nuclei.

38

39 **Keywords:** corticopontine topography, layer V neurons, area mapping genes, *Nr2f1*, mouse  
40 models, *Thy1-eYFP-H* reporter line, pontine nuclei, 3D data points, interactive 3D viewer tools,  
41 anterograde fluorescent tracing

## 42 INTRODUCTION

43 Neuronal populations responsible for fine motor coordination are arranged in topographically  
44 organized maps in the neocortex and cerebellum exemplified by different body parts being  
45 represented in largely continuous maps in the somatosensory cortex (Chapin and Lin, 1984,  
46 Fabri and Burton, 1991, Welker, 1971, Woolsey and Van der Loos, 1970), and discontinuous,  
47 fractured maps in the cerebellum (Bower et al., 1981, Bower, 2011, Leergaard et al., 2006,  
48 Bower and Kassel, 1990, Nitschke et al., 1996, Shambes et al., 1978). The intercalated regions  
49 of this network, including the pontine nuclei, deep cerebellar nuclei, and the thalamus,  
50 receive and integrate signals ultimately resulting in coordinated and seamlessly executed  
51 behaviors (Peterburs and Desmond, 2016, Buckner, 2013, Stoodley and Schmahmann, 2010),  
52 including fine voluntary movements (Badura et al., 2013, Mottolese et al., 2013).

53 The pontine nuclei constitute the major synaptic relay for cerebro-cerebellar signals (Brodal  
54 and Bjaalie, 1992, Lemon, 2008, Mihailoff et al., 1985). Axonal projections originating from  
55 layer V pyramidal neurons across the neocortex are distributed in topographically organized  
56 clusters within the pontine nuclei, as shown in monkey (Brodal, 1978, Schmahmann and  
57 Pandya, 1997), cat (Bjaalie and Brodal, 1997), rat (Leergaard et al., 2000a, Leergaard et al.,  
58 2000b), and to some extent also in mice (Henschke and Pakan, 2020, Inoue et al., 1991,  
59 Proville et al., 2014). Within the pontine nuclei, the three-dimensional (3D) arrangement of  
60 clustered terminal fields, well described in rats, both preserves the overall topographical  
61 relationships of the cortical maps, but also partially overlap and introduce new spatial  
62 proximities among projections from different cortical areas (Leergaard, 2003, Leergaard and  
63 Bjaalie, 2007, Bjaalie and Brodal, 1989).

64 To date, the mechanisms responsible for establishing the topographic map between the  
65 neocortex and pontine nuclei are poorly understood. The leading proposition, referred to as  
66 chrono-architectonic hypothesis, postulates that the complex 3D topography is a product of  
67 straightforward spatio-temporal gradients, possibly combined with non-specific chemo-  
68 attractive mechanisms (Altman and Bayer, 1996, Leergaard, 2003, Leergaard and Bjaalie,  
69 2007, Leergaard et al., 1995). Recent new discoveries open the possibility that other  
70 mechanisms are also in action during the establishment of the corticopontine maps. Several  
71 lines of evidence point to a functional role of gradients in gene expression during topography

72 of sensory maps in several systems (D'Elia and Dasen, 2018, Erzurumlu et al., 2010, Fritzscht  
73 et al., 2019, McLaughlin and O'Leary, 2005), but whether this process is also operative during  
74 establishment of corticopontine topography is not completely understood. A recent study has  
75 shown that postmitotic graded expression of the HOX gene *Hoxa5* is directly involved in  
76 imparting an anterior to posterior identity to pontine neurons, (Maheshwari et al., 2020),  
77 suggesting that pontine nuclei could play an instructive and attractive role in establishing  
78 corticopontine topographical organization. Whether expression in gradients of molecular  
79 factors along the antero-posterior (AP) or medio-lateral (ML) axes of the cerebral cortex also  
80 contributes to determine the topography of corticopontine projections is still not known.  
81 Layer V neurons from the anterolateral cerebral cortex project to the central regions of the  
82 pontine nuclei, while more medially located cortical regions project to more external parts;  
83 projections from motor areas are distributed more medially and rostrally, with projections  
84 from somatosensory areas reaching the middle and caudal parts of the pontine nuclei. Finally,  
85 auditory and visual cortical projections innervate the dorsolateral regions of the pontine  
86 nuclei (Leergaard et al., 2004, Leergaard and Bjaalie, 2007). The fine-tuned and precise  
87 topography between the cortex and pontine nuclei leaves open the possibility for cortical  
88 neurons being intrinsically programmed to target specific groups of pontine neurons, possibly  
89 coupling intrinsic (cell-type specification) and extrinsic (chemo-attractive) mechanisms in  
90 directing proper topographical innervation to the pontine nuclei.

91 Area mapping genes are expressed in gradients along the different axes of the cortical  
92 primordium and known to modulate the size and position of future cortical areas (Alfano and  
93 Studer, 2012, Cadwell et al., 2019, O'Leary and Sahara, 2008). These genes are therefore good  
94 candidates for modulating topographic mapping. In mice, the *Nr2f1* gradient expression  
95 appears to be a particularly strong candidate for having a formative role during the  
96 establishment of topographic maps (Armentano et al., 2007, Zhou et al., 2001, Liu et al.,  
97 2000). For instance, *Nr2f1* (also known as COUP-TFI) is expressed in cortical progenitor cells  
98 from embryonic day E9.0 in a high caudo-lateral to low rostro-medial gradient fashion, and  
99 the gradient expression is maintained in postmitotic descendants as well as postnatally when  
100 the cortical area map is completed (Bertacchi et al., 2019, Flore et al., 2017, Tomassy et al.,  
101 2010). We thus hypothesized that *Nr2f1* could represent one of these factors able to control  
102 topographic corticopontine mapping during corticogenesis.

103 To test this hypothesis, we made use of cortico-specific *Nr2f1* conditional knockout mice as  
104 an *in vivo* model system and a paradigm to investigate the contribution of cortical genetic  
105 programs in the establishment of topographic corticopontine projections. Two distinct  
106 conditional mouse lines, in which *Nr2f1* is knocked out in either cortical progenitor cells or  
107 postmitotic cortical neurons (Alfano et al., 2014, Armentano et al., 2007) were crossed to the  
108 *Thy1-eYFP-H* reporter line (Feng et al., 2000), in which YFP is highly expressed in cortical layer  
109 V pyramidal neurons and their axonal projections (Porrero et al., 2010). The distribution of  
110 fluorescent YFP signals as well as anterogradely labelled corticopontine projections were  
111 evaluated by side-by-side comparison of spatially corresponding microscopic images of  
112 conditional knock-out and control animals, and by 3D visualization of extracted point-  
113 coordinated data representing labelling. Our data indicate that cortical *Nr2f1* expression plays  
114 a dual role in controlling the spatio-temporal development of corticopontine projections.  
115 While early expression in progenitor cells influences the ratio between corticofugal fibers  
116 passing the pontine nuclei, thus precluding any topographic function, loss of solely  
117 postmitotic late expression specifically affects topographic pontine mapping. Overall, our  
118 results demonstrate that intrinsic genetic programs and postmitotic graded expression of  
119 cortical area mapping genes are implicated in the spatio-temporal establishment of area-  
120 specific targeting of corticopontine neurons.

## 121 RESULTS

### 122 Benchmark 3D topographic organization of corticopontine projections in wild-type mice

123 To first establish a 3D reference of the topographical organization of corticopontine  
124 projections in normal adult mice, we used tract tracing data from the *Allen Institute Mouse*  
125 *Brain Connectivity Atlas* (Wang et al., 2020) to visualize the spatial distribution of the pontine  
126 projections of motor and somatosensory neocortical areas. **Figure 1** shows a flowchart of the  
127 different processing and analytic steps used for the different animal groups. Before evaluating  
128 the YFP signal in the cortex, pontine nuclei, and medulla oblongata of *Nr2f1* mutant mice, we  
129 first determined the normal topographical organization of motor and somatosensory  
130 corticopontine projections in wild-type mice. We semi-quantitatively recorded anterogradely

131 labelled corticopontine projections from microscopic images as 3D data points that were co-  
132 visualized in a 3D viewer tool (**Figure 2**).

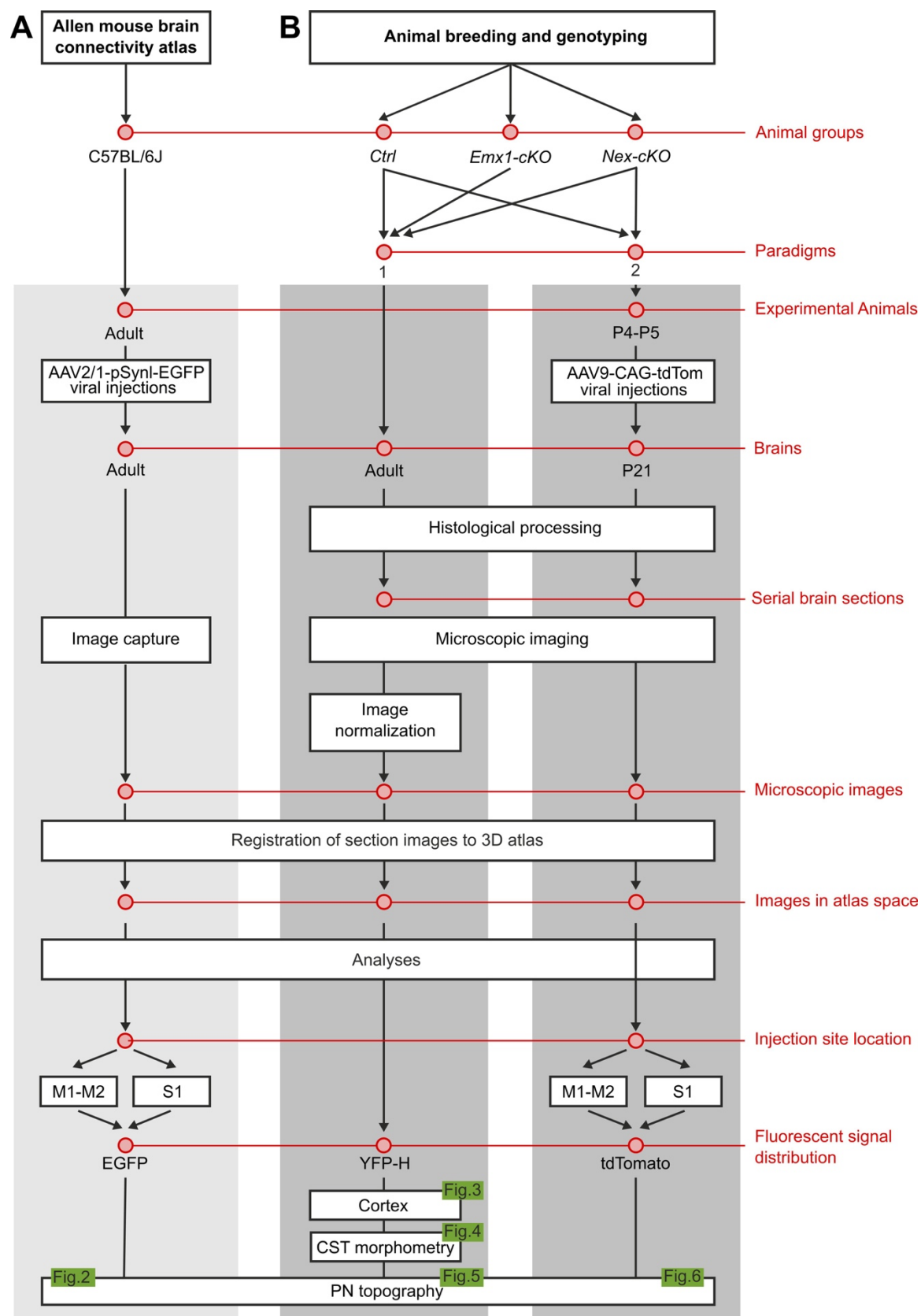
133 3D visualization of data points representing corticopontine labelling arising from two similarly  
134 located tracer injections in the S1 face representation in C57BL/6J wild-type mice from the  
135 *Allen Mouse Brain Connectivity* (**Figure 2A-E**), and our control mice (**Figure 2F-J**), showed  
136 similar distributions of labelling in the central core of the pontine nuclei, resembling the  
137 distribution of corticopontine projections from the somatosensory face region reported  
138 earlier in rats (Leergaard et al., 2000b). Comparison of data points representing  
139 corticopontine projections from different locations across the primary/secondary motor  
140 cortex (M1, M2; n = 6) and primary somatosensory cortex (S1; n = 5) in wild type mice, showed  
141 that motor and somatosensory corticopontine projections target largely segregated  
142 subspaces of the pontine nuclei, with somatosensory projections located predominantly in  
143 central and caudal parts, while projections originating from the motor cortex were located  
144 more rostrally and ventrally, partly surrounding the sensory projections externally (**Figure 3A-**  
145 **G**).

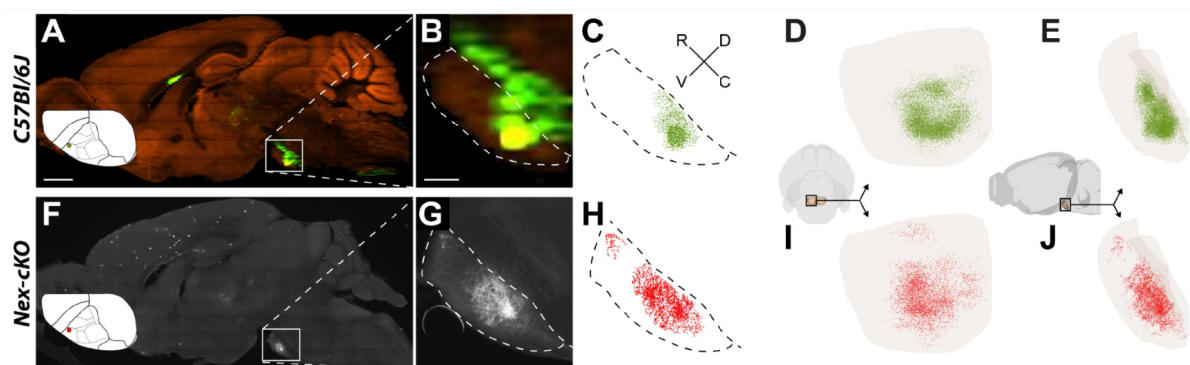
146

147

148 **Figure 1. Experimental and analytic workflow.** The three columns represent workflow steps, with logic and  
149 outputs, followed to investigate topographical organization in the different experimental paradigms. (A)  
150 The left column represents the workflow for generating a 3D control topographic map of corticopontine  
151 projections using public tract tracing data (<https://connectivity.brain-map.org/>), mapped and compared in  
152 a 3D reference atlas space. (B) The middle and right column represent the two paradigms investigated in  
153 conditional mouse models, with the analytic steps performed in adult control, *Emx1-cKO* and *Nex-cKO*  
154 mutant animals (middle column, paradigm 1), and the tract tracing study of the 3D topography of motor  
155 and somatosensory corticopontine projections in young control and *Nex-cKO* mutant animals (right column,  
156 paradigm 2). All images were spatially registered to the Allen mouse brain atlas (CCFv3; Wang et al., 2020)  
157 prior to analyses, to facilitate comparison of images and spatial distribution patterns. Results are shown in  
158 Figures 2-7.

159





161

162

163

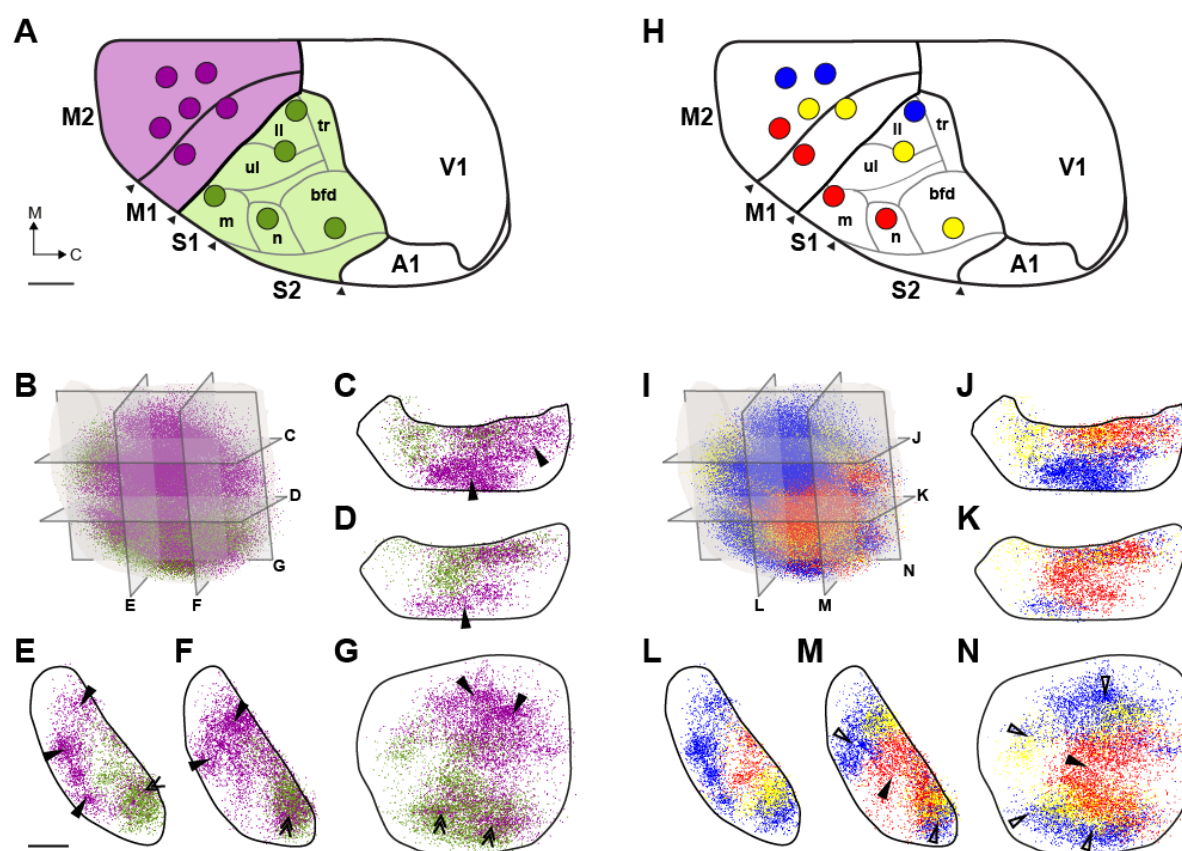
164 **Figure 2. Semi-quantitative recording and 3D visualization of corticopontine tracing data.** Examples  
165 illustrating the data acquisition of corticopontine projections labelled by viral tracer injection in the S1 face  
166 representation in C57BL/6J mice from the Allen Mouse Brain Connectivity Atlas (A-E), and control mice from  
167 the present study (F-J). Panels A,B and F,G show anterogradely labelled axons observed by fluorescence  
168 microscopy in two sagittal sections through the right pontine nuclei. C and H indicate semi-quantitatively  
169 recorded point corresponding to the observed density of labelling observed in B and G. Panels D,E and I,J  
170 show the 3D point populations recorded in each case together with a transparent surface rendering of the  
171 right pontine nuclei, seen from ventral (D,I) and medial (E,J) views, as indicated in the 3D inset. In both  
172 cases, the S1 corticopontine projections are distributed in dense clusters located centrally in the pontine  
173 nuclei. Abbreviations: C, caudal; D, dorsal, R, rostral, V, ventral. Scale bars, 1 mm (A,B) and 200  $\mu$ m (B,G).

173

174 To further test whether motor and somatosensory corticopontine projections follow the  
175 topographical distribution principles as described in rats (Leergaard and Bjaalie, 2007), we  
176 selected experiments with tracer injections located progressively more medially and caudally  
177 in the cerebral cortex (Figure 3H), following the cortical neurogenetic gradient that ripples  
178 out from the anterolateral cortex (Smart, 1984, Leergaard and Bjaalie, 2007). The 3D  
179 visualizations shows that mouse corticopontine projections are concentrically organized, with  
180 projections from the anterolateral neocortex located centrally in the pontine nuclei, and  
181 projections from more medially located parts of somatosensory and motor cortex distributed  
182 in progressively more peripheral parts of the pontine nuclei, and attaining a circular shape  
183 surrounding the central core (Figure 3I-N), in agreement with topographical distribution  
184 principles shown in rats (Leergaard and Bjaalie, 2007). Taken together, our findings confirm  
185 that the somatosensory and motor neurons of the mouse cortex project to largely separate  
186 parts of the pontine nuclei (Henschke and Pakan, 2020, Inoue et al., 1991, Proville et al.,  
187 2014), with clustered terminal fields that are topographically distributed in the same  
188 concentric fashion as previously shown in rats (Leergaard et al., 2000a, Leergaard and Bjaalie,  
189 2007). The 3D point data presented here are also used below as supplementary control data,



190 and as benchmarks for interpreting YFP expression and tract-tracing results in *Nr2f1* mutant  
 191 mice.



192  
 193 **Figure 3. Topographical organization of corticopontine projections in wild-type mice.** 3D visualizations of  
 194 point clouds representing spatial distribution of anterogradely labeled corticopontine axons in wild-type  
 195 mice from the Allen Mouse Brain Connectivity Atlas, injected with the anterograde tracer EGFP in the  
 196 primary (M1)/secondary (M2) motor cortex or primary somatosensory (S1) cortex, at locations indicated  
 197 with color coded circles in A and H. (B, I) 3D visualizations of axonal labelling semi-quantitatively  
 198 represented by points, inside a surface rendering of the outer boundaries of the right pontine nuclei  
 199 (transparent grey surface) shown ventrally. A grid of transparent grey planes with sagittal, transversal, and  
 200 frontal orientation, relative to the pontine nuclei, indicate the position and orientation of ~100  $\mu$ m thick  
 201 digital slices cut through the point clouds, shown in C-G, and J-N. (B-G) 3D co-visualization of all data points  
 202 representing corticopontine projections from the 11 cases, with purple points representing projections from  
 203 M1/M2, and green points representing projections from S1. The slices through the point clouds show that  
 204 motor and somatosensory areas largely target different parts of the pontine nuclei, with projections from  
 205 M1 and M2 located more peripherally towards rostral, ventral, and medial than projections from S1  
 206 (arrowheads in C-G), but also that motor and sensory projections overlap caudally in the pontine nuclei  
 207 (double arrowheads in E-G). (I-N) 3D co-visualization of all data points from the 11 cases, color coded in red,  
 208 yellow or blue according to the location of the cortical injection sites from anterolateral (red) progressively  
 209 towards medial or posterior (yellow, blue). The slices through the point clouds reveal a concentric  
 210 arrangement in the pontine nuclei, with projections from the anterolateral parts of the M1/M2 and S1  
 211 located centrally and medially (arrowheads in M, N), and projections from more medial and posterior  
 212 cortical locations progressively shifted towards rostral, caudal, and lateral (unfilled arrowheads in (M,N)).  
 213 Abbreviations: A1, primary auditory cortex; bfd, barrel field; ll, lower limb; m, mouth; M1, primary motor  
 214 cortex; M2, secondary motor cortex; n, nose; S1, primary somatosensory cortex; S2, secondary  
 215 somatosensory cortex, tr, trunk; ul, upper limb. Scale bars, 1 mm (A,H), 200  $\mu$ m (B-G, I-N).

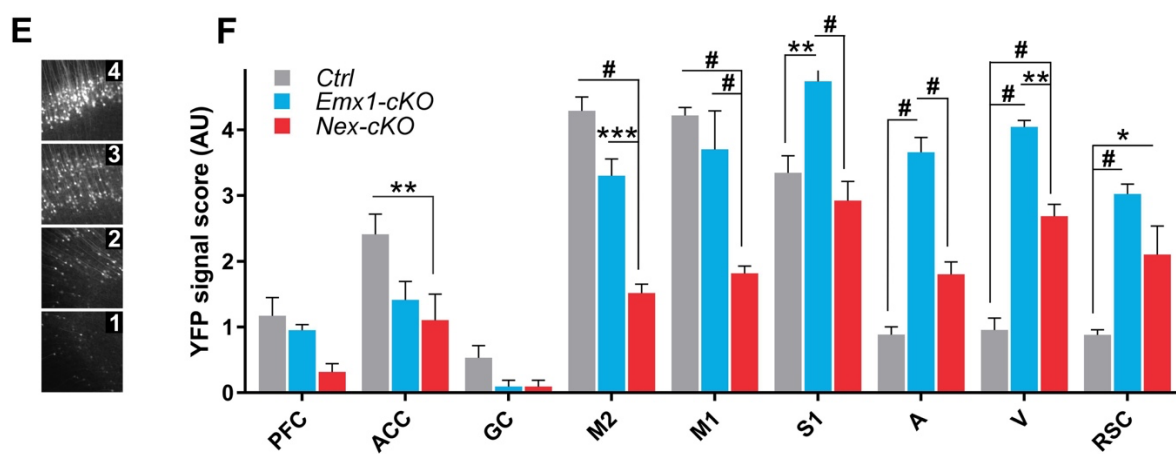
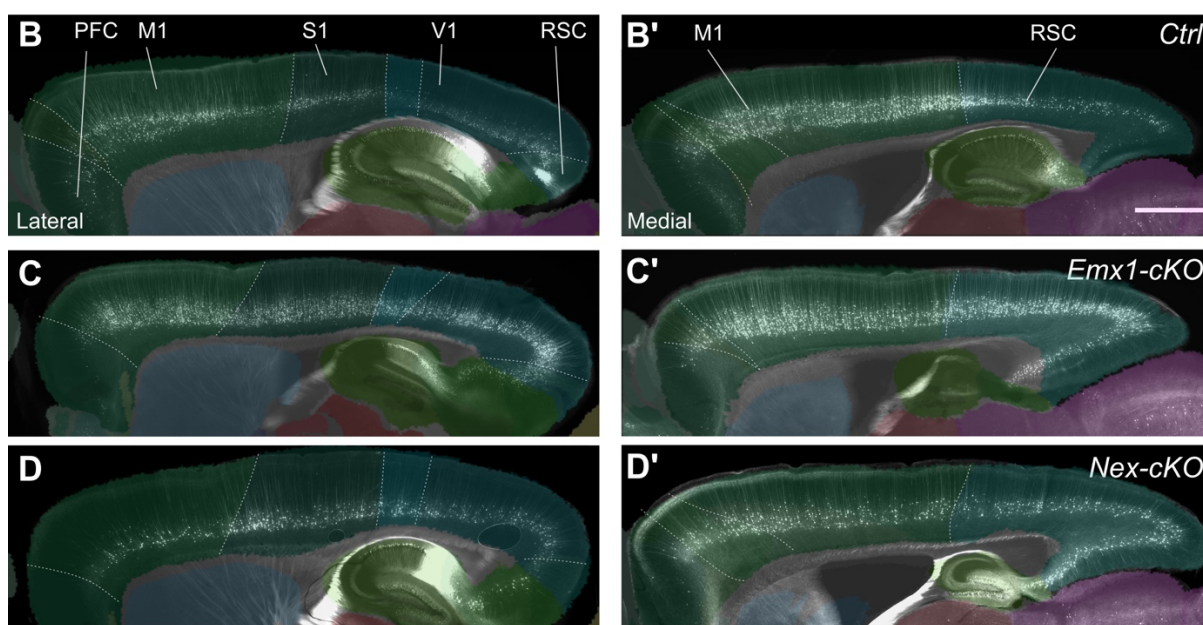
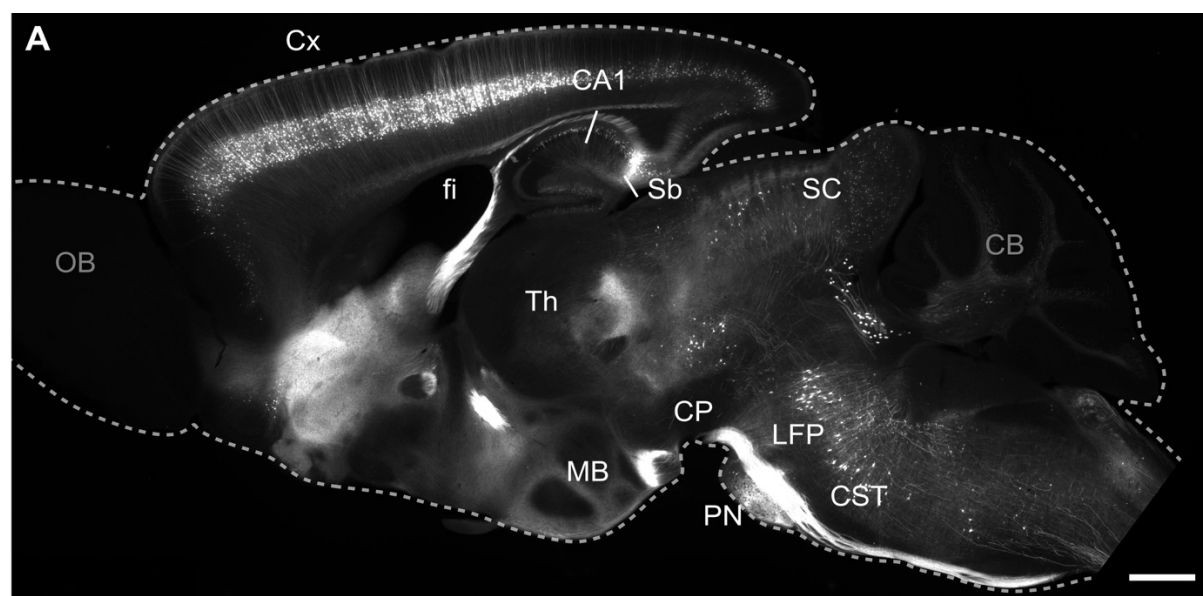
## 216 **Different area-specific layer V neuron distribution in cortices lacking Nr2f1**

217 To assess the influence of cortical area mapping on the establishment of topographical  
218 organization in mouse corticopontine projections, we used as experimental model systems  
219 *Nr2f1* deficient mice (Alfano et al., 2014, Armentano et al., 2007), and first investigated the  
220 spatial organization of layer V cortical distribution and corticopontine axonal projections in  
221 mutant adults compared to control animals. To this purpose, we used two well-established  
222 conditional *Nr2f1* mouse mutants: the *Nr2f1<sup>fl/fl</sup>::Emx1-Cre* mouse, in which *Nr2f1* expression  
223 is abolished from early cortical progenitor cells at mouse embryonic (E) age 9.5 (Armentano  
224 et al., 2007), and the *Nr2f1<sup>fl/fl</sup>::Nex-Cre* mouse in which *Nr2f1* expression is inactivated at later  
225 stages (E11.5-E12), solely in cortical postmitotic neurons (Alfano et al., 2014, Goebbels et al.,  
226 2006). Both mouse lines were crossed to the *Thy1-eYFP-H* reporter line to specifically restrict  
227 signal expression to the majority of layer V pyramidal neurons, allowing labelling of  
228 subcortical projection neurons, including corticospinal and corticopontine fibers (Harb et al.,  
229 2016, Porrero et al., 2010). For simplicity, both lines will be named from here on *Emx1-cKO*  
230 and *Nex-cKO*, respectively.

231 In agreement with the earlier detailed report by Porrero et al. (Porrero et al., 2010), we  
232 observed substantial YFP signal expression in the hippocampus, tectum, and pontine nuclei,  
233 as well as in the globus pallidus, claustrum, endopiriform nucleus, nucleus of the lateral  
234 olfactory tract, mammillary nuclei, piriform area, and the substantia innominata in adult mice  
235 (**Figure 4A**). Signal expression was also seen in the vestibular nuclei, deep cerebellar nuclei,  
236 and cerebellum. Although signal expression was present in almost the same regions in 2-  
237 months-old mutant mice as in controls, more detailed analysis of signal expression in  
238 neocortical areas revealed some distinct differences in the spatial distribution of *Emx-cKO* and  
239 *Nex-cKO* brains relative to their respective controls, and between the two conditional lines.  
240 We used a semi-quantitative scoring system to estimate the amount of signal expression  
241 across the cerebral cortex, in areas defined by delineations derived from spatially registered  
242 overlay images from the *Allen Mouse Brain Atlas* ((Wang et al., 2020); **Figure 1; Figure 4B-D'**).  
243 In control animals, the distribution of YFP-expressing neurons followed a rostrally high to  
244 caudally low gradient (**Figure 4A, B, B'**), in line with the strong YFP signal in layer V neurons  
245 of M1 and S1 areas known to contain representations of the trunk and limbs and to the earlier

246 documented high numbers of layer V neurons in the rostrally located motor areas (Polleux et  
247 al., 1997, Shepherd, 2009, Porrero et al., 2010). Strong staining in these areas resulted in  
248 bright signal expression in the cerebral peduncle and CST (**Figure 4A**). Notably, in the cortex  
249 of mutant animals, this gradient was disrupted and the YFP signal more homogenously  
250 distributed along the anteroposterior axis and at both lateral and medial levels (**Figures 4C,**  
251 **C' and D, D'**). Increased YFP expression was observed caudally in the occipital and  
252 retrosplenial cortex in both groups of mutant mice, in conjunction with decreased YFP signal  
253 in frontal areas, which was particularly more pronounced in *Nex-cKO* than *Emx1-cKO* mice  
254 (**Figures 4B-F**). Interestingly, the highest signal of YFP expression was observed in the *Emx1-*  
255 *cKO* S1 cortex (**Figure 4B, C, F**), but no statistical difference compared to controls was  
256 detected in S1 of *Nex-cKO* brains (**Figure 4B, D, F**). Together, these data indicate a different  
257 role for Nr2f1 in early progenitor cells (*Emx1-cKO*) and late postmitotic neurons (*Nex-cKO*)  
258 during layer V differentiation, as assessed by YFP signal expression, across all cortical areas,  
259 particularly in M1 and S1 (**Figure 4F**).

260  
261 **Figure 4 – Cortical distribution of YFP-positive layer V pyramidal neurons in control, *Emx1-cKO* and *Nex-***  
262 ***cKO* adult brains. (A) Fluorescence microscopy image of a representative sagittal section from a *Thy1-YFP-***  
263 ***H* mouse brain, showing widespread YFP expression. (B-D/B'-D')** Fluorescence microscopy images from  
264 sagittal sections located laterally (**B-D**) and more medially (**B'-D'**) in Ctrl, *Emx1-cKO*, and *Nex-cKO* brains,  
265 with custom made, spatially corresponding CCFv3 atlas diagrams superimposed on the microscopic images  
266 to define the location of different cortical areas. (E) Semi-quantitative scale used to score the amount of  
267 signal expression: 0, attributed to absence of positive cells (not shown); 1, very few and sparse cells with  
268 low to medium signal intensity; 2, moderate number of sparse cells with moderate to high signal intensity;  
269 3, high number of partially overlapping cells with high signal intensity; 4, very high number of extensively  
270 overlapping cells with high to very high signal intensity. (F) Column graphs showing the scoring of YFP-H  
271 signal expression across cortical areas in adult Ctrl (grey), *Emx1-cKO* (light blue) and *Nex-cKO* (red) mice. In  
272 *Emx1-cKO* samples, less signal expression is seen in the most anterior regions (ACC and M2, but not M1),  
273 whereas increased signal is quantified in parietal and occipital regions (S1, A, V. and RSC), relative to the  
274 control condition. In *Nex-cKO* animals, the amount of signal is reduced in ACC, M2 and M1, with no  
275 statistical difference in S1 compared to controls, but with increased amount of signal in A, V, and RSC, even  
276 if lower than in *Emx1-cKO*s. \* < 0.05, \*\* < 0.01, \*\*\* < 0.005, # < 0.0001. Data are represented as mean ± SEM.  
277 Data were analyzed with 2way-ANOVA test and corrected for multiple comparison with the Bonferroni test  
278 (see also **Supplementary Table 4**). Ctrl, n=6; *Emx1-cKO*, n=4, *Nex-cKO*, n=4.. Abbreviations: A, auditory  
279 cortex; ACC, anterior cingulate cortex; CA1, cornu ammonis area 1; CB, cerebellum; CP, cerebral peduncle;  
280 CST, corticospinal tract; Cx, cortex; fj, fimbria; GC, gustatory cortex; LFP, longitudinal fascicle of the pons;  
281 M1, primary motor cortex; M2, secondary motor cortex; MB, mammillary body; OB, olfactory bulb; PFC,  
282 prefrontal cortex; PN, pontine nuclei; RSC, retrosplenial cortex; S1, primary somatosensory cortex; SC,  
283 superior colliculus; Sb, subiculum; Th, thalamus; V, visual cortex. Scale bars: 1000µm (**A**); 500µm (**B-D; B'-**  
284 **D'**).  
285

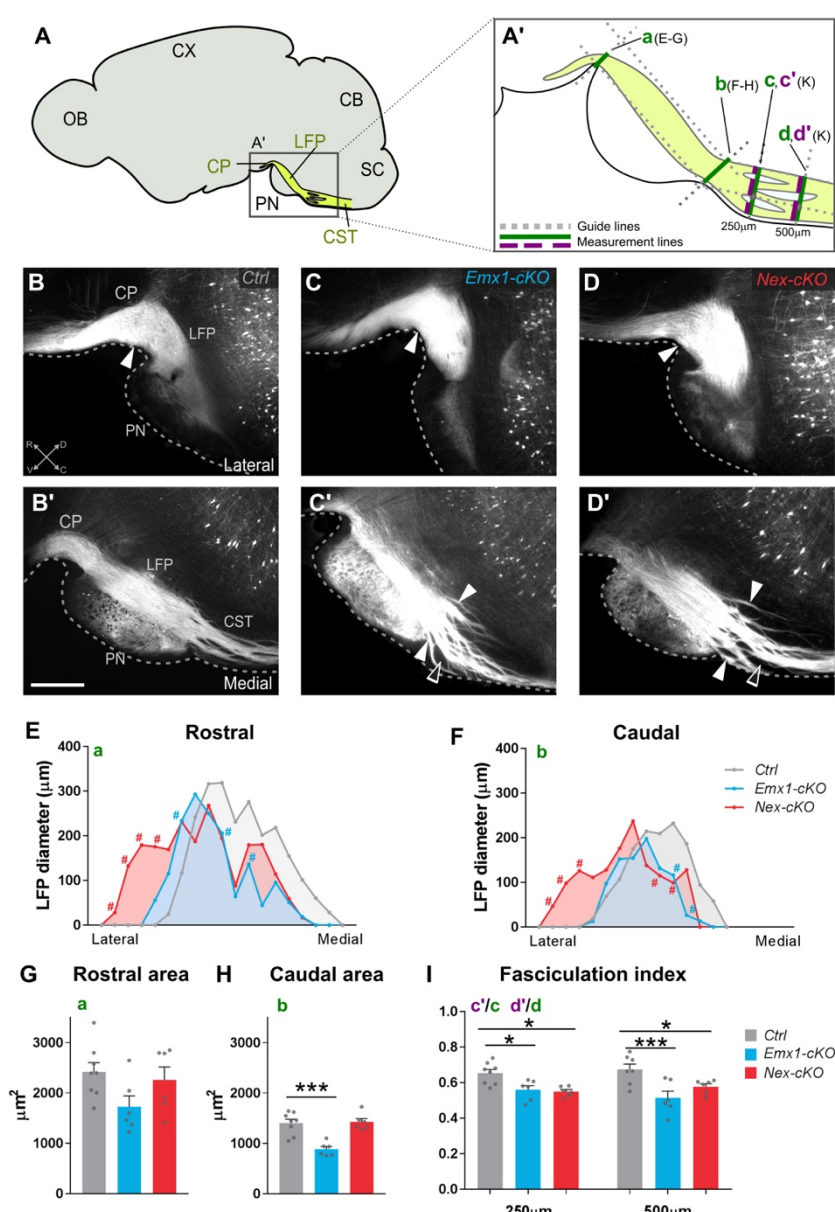


## 287 **Abnormal corticospinal projections and fasciculation in *Nr2f1* mutant brains**

288 Next, we asked whether the impaired cortical distribution of YFP expressing layer V neurons  
289 in mutant mice influences the integrity of subcortical axonal projections. In all cases (mutant  
290 and controls alike), strong YFP signal expression was seen bilaterally in the main corticofugal  
291 pathways (**Figure 4A**), visible as longitudinally oriented fiber bundles coursing through the  
292 caudoputamen towards the cerebral peduncle (**Figure 5A-D**), passing dorsal to the pontine  
293 nuclei as the longitudinal fasciculus of the pons (**Figure 5B'-D'**), and continuing through the  
294 brain stem towards the spinal cord as the CST. Since a large fraction of the corticobulbar fibers  
295 terminate in the pontine nuclei (Tomasch, 1969, Tomasch, 1968), we hypothesized that  
296 abnormal distribution of YFP-expressing layer V neurons observed in mutant mice (**Figure 4**)  
297 might affect corticopontine innervation, and could be reflected in an abnormal size of the  
298 pontine longitudinal fascicle as it enters the cerebral peduncle and exits the pons in rostral  
299 and caudal positions to the pontine nuclei, respectively. To evaluate this, we measured the  
300 dorsoventral width of the longitudinal fascicle of the pons in sequential sections along the  
301 medio-lateral axis. The measurements were taken at rostral and caudal levels to the pontine  
302 nuclei in the three genotypes (**Figure 5A'**). Surprisingly, we found the lateral part of the  
303 fascicle to be wider at both rostral and caudal levels in *Nex-cKO* mice compared to *Emx1-cKO*  
304 and controls, while being narrower medially (see red area chart in **Figure 5E, F**). This suggests  
305 that the longitudinal fascicle of the pons is flattened and expanded laterally upon *Nr2f1*  
306 inactivation in postmitotic neurons. Smaller differences were observed in the *Emx1-cKO*  
307 fascicle which shape was however more similar to controls than to the *Nex-cKO* one (blue  
308 area chart in **Figure 5E, F**). This is also supported by quantification of the total surface of the  
309 longitudinal fascicle of the pons at rostral and caudal levels, which shows a significant surface  
310 reduction at caudal but not rostral levels in *Emx1-cKO* mice (**Figure 5G, H**). These data indicate  
311 that loss of *Nr2f1* in progenitors results in fewer YFP-expressing fibers passing the pontine  
312 nuclei towards the brain stem to form the CST.

313 Moreover, we observed, caudal to the pontine nuclei, abnormally widespread fiber fascicles  
314 in the CST of mutant animals (arrowheads in **Figure 5C', D'**). To determine whether this was  
315 a significant difference between animal groups, we estimated the degree of fiber bundle  
316 fasciculation in the CST of *Emx1-cKO* and *Nex-cKO* mice. At locations of 250 $\mu$ m and 500 $\mu$ m

317 caudal to the pontine nuclei (**Figure 5A'**), we measured the total dorsoventral width of the  
 318 CST at several mediolateral levels and subtracted the width of gaps between the YFP-  
 319 expressing fiber bundles at the same levels. The ratio of the total width of the CST and width  
 320 of the fibers only was used as a measure of the fasciculation index (**Figure 5I**). Notably, in both  
 321 groups of mutant mice we found a lower degree of fasciculation in the CST which was more  
 322 pronounced at the most caudal level (**Figure 5I**). Together, these data show that *Nr2f1*  
 323 expression (both in cortical progenitor cells and postmitotic cells) controls the diameter,  
 324 shape and degree of fasciculation of the CST originating from layer V neurons.



325  
 326 **Figure 5 – Loss of *Nr2f1* function leads to abnormal corticospinal projections and fasciculation.** (A)  
 327 Schematic diagram of a sagittal mouse brain section showing the location of the pontine nuclei (PN) and

328 descending fiber tracts (yellow) in the cerebral peduncle (CP), longitudinal fascicle of the pons (LFP) and  
329 corticospinal tract (CST) at level of the pons. (A') Diagram taken from A illustrating the different  
330 measurements shown in E-I. The frame reflects the region shown in B-D and B'-D' in control (Ctrl), *Emx1-*  
331 *cKO* and *Nex-cKO* animals. (B-D) Lateral sagittal section showing the corticospinal tract entering the pons  
332 level as a continuation of the cerebral peduncle. White arrowheads point to the site of measurement plotted  
333 in E, showing a similar thickness of the bundle in the three genotypes. (B'-D') Medial sagittal section  
334 showing the corticospinal tract passing dorsal to the pontine nuclei and defasciculating prior to entering  
335 the spinal cord. Full arrowheads point to fiber bundles (thinner and more dispersed in both *Emx1-cKO* and  
336 *Nex-cKO* mutants), empty arrowheads point to empty spaces between bundles. (E, F) Plots showing LFP  
337 diameter measurements obtained from lateral to medial before and after innervating the pontine nuclei  
338 (rostral and caudal respectively) for the three genotypes. Each measurement represents the average value  
339 of corresponding sections among distinct animals and each position on the x-axis represents a specific  
340 section of the series. (G-H) Column graphs showing average values of the area under the curves in E-F. A  
341 comparable number of fibers reach the cerebral peduncle in the three genotypes (G). In *Emx1-cKO* brains  
342 fewer fibers are seen to exit the level of the pons compared to control- and *Nex-cKO* brains (H). (I) Column  
343 graph showing CST fasciculation index, based on measurements of total thickness and fiber thickness (green  
344 and purple line respectively in A') performed at 250 and 500  $\mu\text{m}$  from the terminal edge of the pontine  
345 nuclei. A ratio between the two measurements was calculated for each position. Data are represented as  
346 mean  $\pm$  SEM. Data were analyzed with 2way-ANOVA test (E-F) or ordinary one-way ANOVA test (G-I) and  
347 corrected for multiple comparison with the Bonferroni test (see also Supplementary Table 4). Ctrl, n=8;  
348 *Emx1-cKO*, n=6; *Nex-cKO*, n=6. #<0.05 (E-F) \* < 0.05, \*\*< 0.01, \*\*\*<0.005 (G-I). Abbreviations: CB,  
349 cerebellum; CP, cerebral peduncle; CST, corticospinal tract; CX, cortex; LFP, longitudinal fascicle of the pons;  
350 OB, olfactory bulb; PN, pontine nuclei; SC, spinal cord. Scale bar=500 $\mu\text{m}$ .

351

## 352 Dual role of Nr2f1 in targeting corticopontine projections

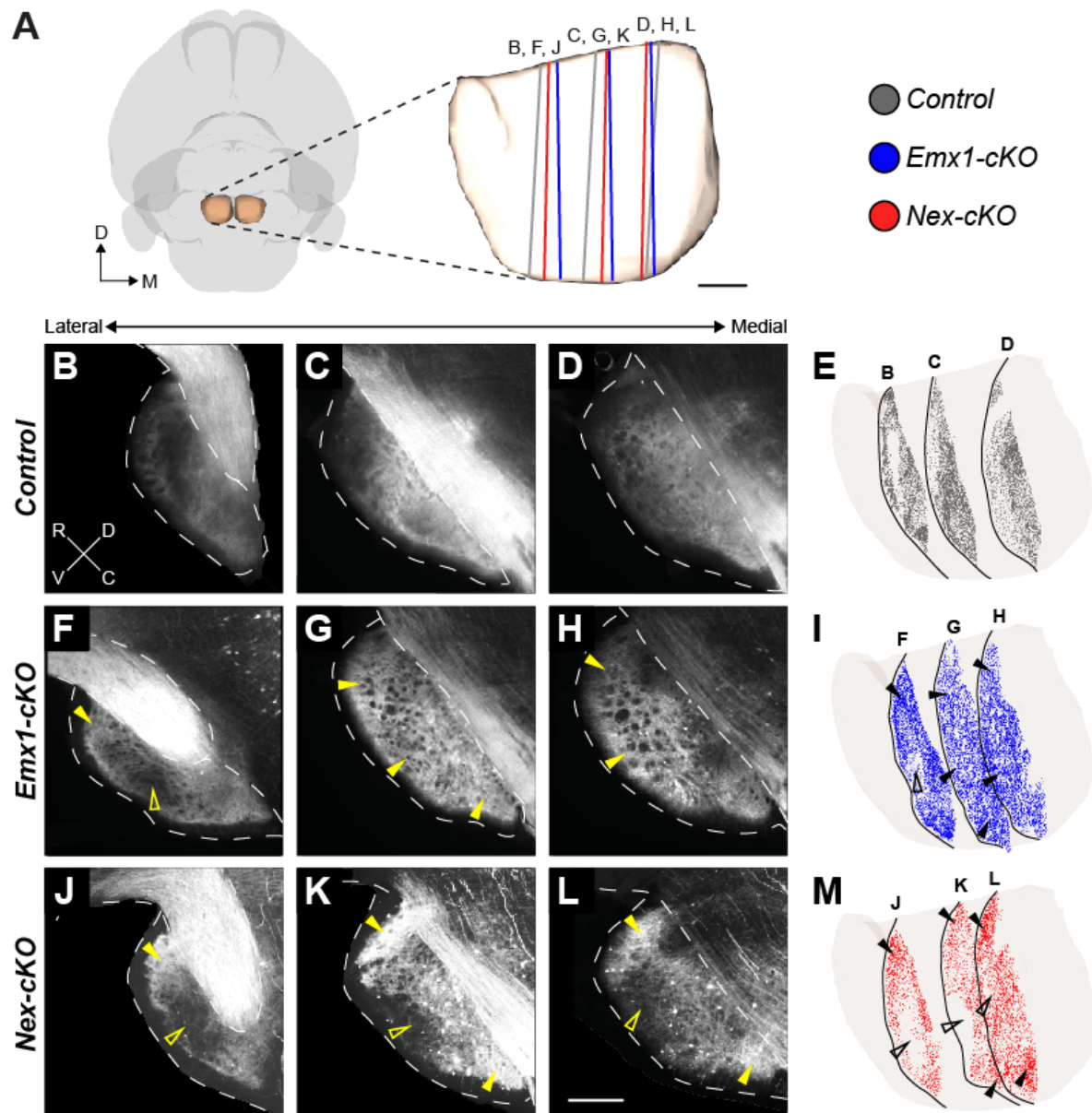
353 To evaluate whether topographical organization of corticopontine projections was dependent  
354 on proper cortical area mapping, we assessed the spatial distribution of YFP signal expression  
355 within the pontine nuclei by comparing intensity-normalized microscopic images of spatially  
356 corresponding sagittal sections from the brains of *Emx1-cKO*, *Nex-cKO* and control animals  
357 (Figure 6A). In all mice, widespread signal expression was seen across most parts of the  
358 pontine nuclei (Figure 6B-L). A complete documentation of spatially comparable images  
359 showing YFP expression in the pontine nuclei of all mutant mice and controls is provided in  
360 Supplementary Figures 1 and 2. In control brains, we observed a strong YFP signal in central  
361 parts of the pontine nuclei, with the densest expression tending to surround a centrally  
362 located zone exhibiting less dense signals (Figure 6B-E). This region of the pontine nuclei  
363 typically receives strong projections from S1 areas (Figure 3). Some signal expression was also  
364 visible in medial parts of the pontine nuclei (Figure 6D, E), which is known to receive  
365 projections from the cortical motor areas (Figure 3). By contrast, signal expression was lower

366 in rostral and lateral parts of the pontine nuclei (**Figure 6B, C, E**), which are known to receive  
367 projections from visual and auditory areas of the cerebral cortex (Inoue et al., 1991, Leergaard  
368 and Bjaalie, 2007).

369 Interestingly, *Emx-cKO* mice showed a relatively homogeneous signal distribution across all  
370 parts of the pontine nuclei, and notably also displayed more signal expression in the  
371 dorsolateral regions (**Figure 6F-I**). Signal expression was also present in the medial part of the  
372 nuclei, albeit with lower density than in the central region (**Figure 6G-I**). This observation fits  
373 well with the finding of more extensive YFP signal expression in the occipital cortex (**Figure**  
374 **4C,C'**), which projects to the dorsolateral pontine nuclei. By comparison, the signal expression  
375 observed in *Nex-cKO* animals was more constrained and predominated in rostrally and  
376 caudally located clusters extending from the cerebral peduncle towards the ventral surface  
377 of the pons, and medially surrounding a central core in which little signal was expressed  
378 (**Figure 6J-M**). These clusters were more peripherally located than the clustered signal  
379 expression observed in control animals (**Figure 6J-M**). Notably, in all *Nex-cKO* cases little signal  
380 expression was seen in the central region of the PN (unfilled arrowheads in **Figure 6J-L**),  
381 despite the presence of YFP-expressing layer V neurons in S1 (**Figure 4D,D, F**). This central  
382 region is normally innervated by projections from the face representations located in S1  
383 (**Figures 2, 3**).

384 Taken together, these findings show that corticopontine projections are abnormally  
385 distributed in *Nr2f1* cortical deficient mice, with more homogenously (non-specifically)  
386 distributed expression in *Emx1-cKO* mice, and more peripherally distributed signal expression  
387 in *Nex-cKO* mice, that display reduced expression in the central region of the pontine nuclei  
388 normally receiving S1 projections. In both mutant groups the signal expression was expanded  
389 to dorsolateral regions of the pontine nuclei that normally are innervated by projections from  
390 occipital cortical areas. This suggests that cortical *Nr2f1* graded expression in postmitotic  
391 neurons is directly involved in the establishment of topographically organized corticopontine  
392 projections.





393

394 **Figure 6. Distribution of YFP signal expression in the pontine nuclei in knock-out mice and controls.** (A)  
 395 3D representation of the outer surfaces of the brain (transparent grey) and pontine nuclei (transparent  
 396 brown) from the Allen mouse brain atlas. Pontine nuclei enlarged in ventral view with colored lines  
 397 representing the location and orientation of the sagittal sections shown in B-M. (B-D, F-H, J-L) Fluorescence  
 398 microscopy images of sagittal sections from corresponding mediolateral levels of the pontine nuclei,  
 399 showing the spatial distribution of YFP signal expression in control, Emx1-cKO, and Nex-cKO mice,  
 400 respectively. (E, I, M) 3D visualization of the transparent external surface of the pontine nuclei in an oblique  
 401 view from ventromedial, with point coded representations of signal expression from the sagittal sections  
 402 shown in B-D, F-H, and J-L, respectively. Filled yellow or black arrowheads point to regions with increased  
 403 signal expression in mutant mice, while non-filled arrowheads indicate regions with decreased signal  
 404 expression. In control mice (B-E), signal expression is primarily seen in central and caudal parts of the  
 405 pontine nuclei, while in Emx1-cKO mice (F-I) signal expression is more widespread and diffuse throughout  
 406 the entire pontine nuclei, including more peripheral parts of the pontine nuclei towards rostral, ventral and  
 407 caudal positions (filled arrowheads in G-I). In Nex-cKO mice (J-M), signal expression is reduced in the central  
 408 core region of the pontine nuclei (non-filled arrowheads in K-M), while being increased in peripheral (rostral  
 409 and caudal) regions of the pontine nuclei. Abbreviations: C, caudal; D, dorsal; M, medial, PN, pontine nuclei;  
 410 R, rostral. Scale bars, 200  $\mu$ m.

## 411 **Altered somatosensory topographic projections in *Nex-cKO* adult mutant mice**

412 In addition to Nr2f1 gradient expression in cortical progenitors and early postmitotic neurons,  
413 high expression in primary sensory areas, in which different sensory surfaces are  
414 topographically organized, is maintained at postnatal stages and still consistent with a high  
415 caudolateral to low anteromedial gradient (**Figure 7A**). To further and directly support our  
416 hypothesis of a cortical influence in topographical pontine mapping, we injected the AAV9-  
417 CAGtdTomato anterograde viral tracer (Pourchet et al., 2021) in motor, lateral or medial S1  
418 cortex of 5 days-old (P5) *Nex-cKO* mice and littermate controls (**Figure 7B**). The mice were  
419 sacrificed at P21 and brain sections analyzed microscopically. All histological sections were  
420 spatially registered to the *Allen Mouse Brain Atlas* (common coordinate framework, CCF3;  
421 (Wang et al., 2020)), and the location of tracer injections sites were mapped in the same atlas  
422 space (**Figure 7B**). For each injection site location in a *Nex-cKO* brain, we selected either the  
423 most corresponding control experiment or wild-type tract-tracing data from the *Allen Mouse*  
424 *Brain Connectivity Atlas* (**Figures 2A-E and 3**), as additional controls.

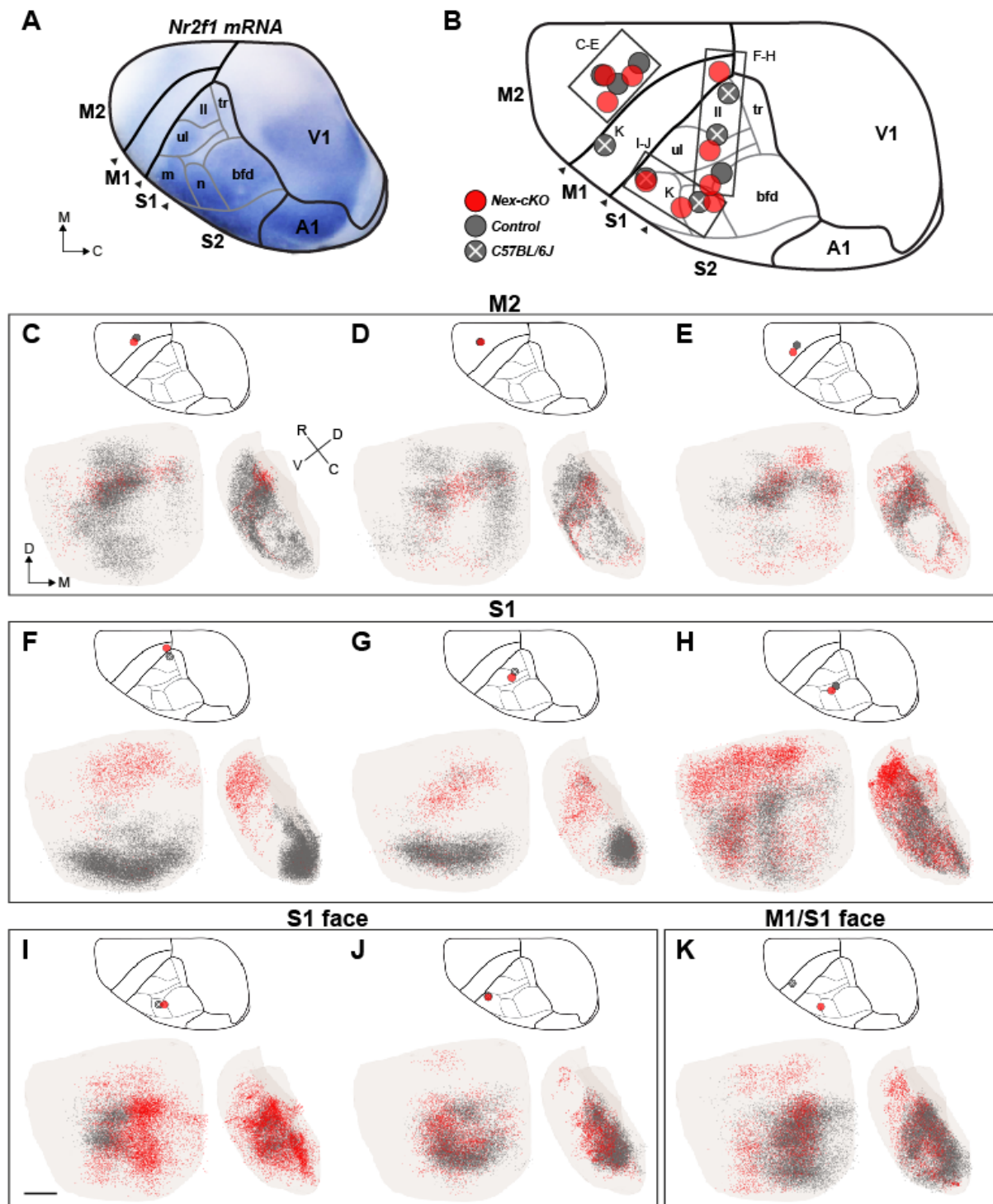
425 In all control mice, the spatial distributions of corticopontine projections (dark gray point  
426 clouds in **Figure 7**) were comparable with the labelling patterns seen in corresponding wild-  
427 type tracing data from the *Allen Mouse Brain Connectivity Atlas*. As expected, tracer injections  
428 into motor areas gave rise to labelled axonal clusters located rostrally, caudally, and medially  
429 in the pontine nuclei (**Figure 7C-E**) or following tracer injection in the head area of M1, in the  
430 medial part of the central core of the pontine nuclei (**Figure 7K**). By contrast, tracer injections  
431 into S1 areas gave rise to labelled axonal clusters located centrally and caudally in the pontine  
432 nuclei (**Figure 7F-J**).

433 In all *Nex-cKO* mice receiving tracer injections into cortical motor areas, the overall  
434 distribution of corticopontine labeling (red point clouds in **Figure 7**) was found to be  
435 essentially like that observed in the control cases (**Figure 7C-E**). By contrast, tracer injections  
436 into S1 representations of the whiskers or upper limb, or into the S1/M1 (sensorimotor) lower  
437 limb representation in *Nex-cKO* brains gave rise to abnormal distribution of corticopontine  
438 fibers (**Figure 7F-I**). Specifically, while the S1 corticopontine projections in wild-type mice  
439 typically form a large, elongated, caudally or laterally located cluster (**Figure 7F-H**, dark grey  
440 points), this labelling was shifted towards more rostral locations in the *Nex-cKO* brains (**Figure**

441 **7F-H**, red points), resembling the distributions observed after tracer injections in motor areas  
442 (**Figure 7C-E**).

443 Notably, tracer injections placed in the anterolateral part of S1 in in *Nex-cko* mice, in regions  
444 representing sensory surfaces of the head, gave rise to labelled axons distributed in the  
445 central part of the pontine nuclei, with more subtle difference to the matching control  
446 experiments (**Figure 7I**). In two cases, projections from the S1 head region were distinctly  
447 shifted towards medial relative to a control experiments (**Figure 7I, and K**), attaining a  
448 distribution resembling the corticopontine projections from head representations in M1  
449 cortex, located significantly more anteriorly in the cortex (**Figure 7K**). These results indicate  
450 that corticopontine projections from the head representations of S1 also display abnormal  
451 topographical distributions resembling the normal projections from homologous  
452 representations in the primary motor cortex. Finally, one tracer injection placed in the most  
453 anterolateral part of S1, representing perioral surfaces in a *Nex-cko* mouse, yielded  
454 corticopontine labelling which was highly similar to that of a control experiment (**Figure 7J**).

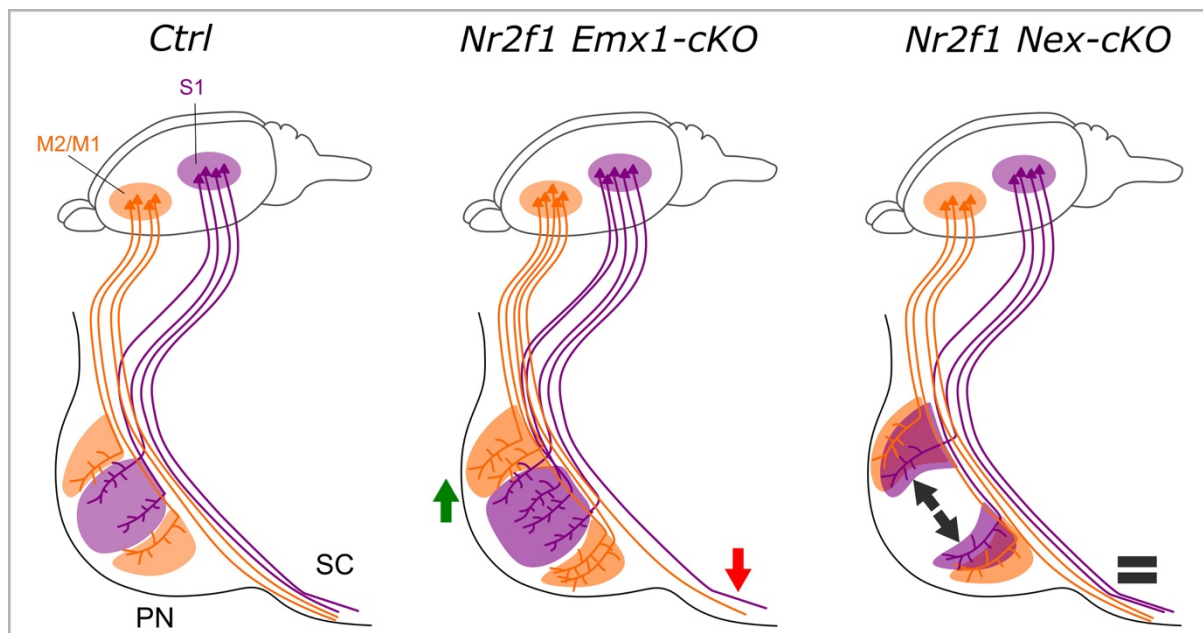
455 Our findings thus show that corticopontine projections from motor areas and the most  
456 anterolaterally located parts of S1 are topographically similar in *Nex-cko* brains and controls,  
457 whereas corticopontine projections from most parts of S1 (head, whisker, upper limb, and  
458 lower limb representations) are abnormally shifted towards rostral and medial regions of the  
459 pontine nuclei, that normally receive projections from cortical motor areas. This is in overall  
460 agreement with the spatial and temporal control of *Nr2f1* in area mapping. Indeed, no  
461 changes in motor-deriving corticopontine projections might be due to low *Nr2f1* expression  
462 in rostral/motor cortex (spatial control), whereas no changes in the projections originating  
463 from the most anterolateral part of S1, the earliest cortical projections to innervate the  
464 forming pontine nuclei, might be explained by the late *Nr2f1* genetic inactivation occurring  
465 after the earliest layer V neurons have been produced (temporal control).



466  
 467 **Figure 7. Anterograde tracing of corticopontine projections from motor and somatosensory areas in Nex-**  
 468 **cKO mice. (A) Dorsal view of a P5 cortical hemisphere positive for *Nr2f1* mRNA transcript, showing graded**  
 469 ***Nr2f1* expression across the right cerebral cortex, with drawings of cortical area representations transferred**  
 470 **from the adult Allen mouse brain atlas. (B) Overview of the location of the anterograde viral tracer injection**  
 471 **sites in the right primary motor (M1), secondary motor (M2), or primary somatosensory (S1) cortex in Nex-**  
 472 **cKO (red), control (dark gray), and wild-type C57BL/6J (dark gray with white cross, data from the Allen**  
 473 **Mouse Brain Connectivity Atlas) brains. (C-J) 3D colored point clouds representing axonal labeling in**  
 474 **corresponding pairs of Nex-cKO (red) or control/wild-type (dark gray) mice, shown within a transparent**  
 475 **surface representation of the right pontine nuclei in ventral and medial views. Inset drawings of the brains**  
 476 **seen from dorsal show the location of tracer injection sites for each combination of point clouds. Tracer**  
 477 **injections in corresponding locations in M2 of both Nex-cKO and control/wild-type mice give rise to quite**

478 similar corticopontine labelling in rostrally located clusters, curving towards ventral and caudal along the  
479 surface of the pontine nuclei (C-E). By contrast, corresponding tracer injections in lower limb and upper limb  
480 representing regions in S1 of Nex-cKO and control/wild-type mice give rise to labelling in different parts of  
481 the pontine nuclei, with corticopontine projections in control mice distributed in elongated curved clusters  
482 located caudally (gray points in F,G) or laterally in the pontine nuclei (gray points in H), while projections  
483 from the same locations in Nex-cKO mice are shifted to more peripheral rostral and lateral parts of the  
484 pontine nuclei (red points in F-H). All tracer injections in the face region of Nex-cKO and control mice gave  
485 rise to labeling in the central region of the pontine nuclei, however with a subtle medial shift of projections  
486 in Nex-cKO brains (I, see also K). Corresponding tracer injections in the most anterolateral part of S1 in a  
487 Nex-cKO and wild-type control gave rise to highly similar labeling, centrally in the pontine nuclei. (K) Tracer  
488 injections in widely separated, homologous locations in S1 (Nex-cKO) and M1 (wild-type control) gave rise  
489 to largely corresponding labeling in the medial part of the central core region of the pontine nuclei, albeit  
490 with additional rostral and medial labelling in the Nex-cKO experiment. This demonstrates that  
491 corticopontine projections from S1 in Nex-cKO mice are changed to resemble normal projections from M2.  
492 Abbreviations: A1, primary auditory cortex; bfd, barrel field; C, caudal; D, dorsal; L, lateral; ll, lower limb;  
493 M, medial; m, mouth; M1, primary motor cortex; M2, secondary motor cortex; n, nose; PN, pontine nuclei;  
494 R, rostral; S1, primary somatosensory cortex; tr, trunk; ul, upper limb. Scale bar, 200  $\mu$ m.

495  
496  
497



498  
499 **Figure 8. Summary schematics of changes in layer V pyramidal neuron connectivity upon cortical Nr2f1**  
500 **inactivation.** In control mice (Ctrl), projections from motor areas (M2/M1, orange) and S1 (purple) target  
501 largely segregated parts of the pontine nuclei, while a substantial amount of fibers continue towards the  
502 spinal cord. Somatosensory projections target the central core region of the PN, while motor projections  
503 target more peripheral rostral, caudal, and medial parts of the pontine nuclei. In Nr2f1 Emx1-cKO mutants,  
504 in which Nr2f1 expression is lost in cortical progenitors and neurons, fewer fibers reach the SC (red arrow)  
505 and more projections target the PN (green arrow), possibly with more diffuse distribution of fibers. In Nr2f1  
506 Nex-cKO animals, in which Nr2f1 expression is inactivated at later stages only in cortical postmitotic  
507 neurons, no difference between corticospinal and corticopontine projections are detected (grey equal sign),  
508 but corticopontine topography of S1 is affected, whereby fibers reach lateral, motor-receiving PN regions  
509 instead of targeting the core (illustrated by grey divergent arrows).  
510

## 511 **DISCUSSION**

512 Our present study questions whether and how spatio-temporal cortical expression gradients  
513 are involved in the establishment of normal topographical organization of corticopontine  
514 projections. By combining genetically modified mice and public mouse brain connectivity  
515 data with tract-tracing techniques and digital brain atlas tools, we have provided novel  
516 evidence of an intrinsic molecular control of layer V cortical neurons during the establishment  
517 of topographical organization of corticopontine projections in a spatial and temporal fashion.  
518 Abnormal areal organization in the neocortex induced by *Nr2f1* inactivation is reflected in  
519 altered corticopontine projections, as well as impaired structural integrity of the CST. While  
520 loss of *Nr2f1* from the early progenitor cell pool leads to increased and abnormal  
521 corticopontine innervation at the expense of corticospinal projections, only late postmitotic  
522 *Nr2f1* inactivation reveals altered topographic pontine mapping from medially located parts  
523 of somatosensory cortex controlling whisker, upper limb, and lower limb representations. No  
524 shifts from motor and somatosensory anterolateral projections were observed in these mice,  
525 in line with a spatial and temporal control of *Nr2f1* expression, respectively. Overall, our data  
526 show that proper area mapping of the neocortical primordium is a pre-requisite for preserving  
527 the cortical spatial and temporal segregation within the pontine nuclei, and thus correct  
528 corticopontine topographic organization.

529

### 530 **Spatial accuracy of topographical data compared across experiments**

531 To ensure proper accuracy of 3D data in wild-type and genetically-modified mice, we relied  
532 on spatial alignment of serial microscopic section images to a common atlas reference space,  
533 achieved through a two-step atlas registration method (Puchades et al., 2019), which included  
534 adjustment of section orientation and non-linear refinement. The process allowed us to  
535 record and compare axonal projections as 3D data points in an interactive viewer tool. The  
536 use of non-linear registration compensated for minor shape differences among brains and  
537 allowed comparison of distribution patterns among spatially relevant data. The focus on the  
538 location rather than the amount of signal expression/axonal labelling also compensated for  
539 the variation in signal expression intensity and size of tracer injections among cases. The

540 approach to comparing axonal distributions as semi-quantitatively recorded data points in 3D  
541 was adopted from well-established methods used in earlier studies of cerebro-cerebellar  
542 organization in rats (Leergaard et al., 2000a, Lillehaug et al., 2002, Leergaard and Bjaalie,  
543 1995, Leergaard et al., 1995, Leergaard et al., 2000b). By representing signal expression and  
544 axonal labeling as 3D point clouds, it became possible to more directly explore and compare  
545 location and distribution patterns in 3D in different combinations of data sets. For the  
546 additional benchmark data extracted from the *Allen Mouse Brain Connectivity Atlas*, we used  
547 the same sagittal image orientation as in our microscopic data, to facilitate comparison of  
548 microscopic images in addition to the 3D comparisons. The relevance and accuracy of the  
549 approach was confirmed by demonstrating that similarly located cortical tracer injections in  
550 control animals gave rise to similarly distributed labelling patterns in the pontine nuclei.

551

## 552 **Area mapping genes and cortical topography**

553 The cortical primordium is initially pre-specified by the combined action of morphogens  
554 secreted by patterning centers that modulate expression gradients of a combination of  
555 transcription factors, largely along three orthogonal (anteroposterior, mediolateral and  
556 dorsoventral) axes (O'Leary and Nakagawa, 2002, Alfano and Studer, 2012). These  
557 transcription factors determine areal fate and regulate expression of downstream molecules  
558 that in turn control the topographic organization of synaptic inputs and outputs of related  
559 structures (Assimacopoulos et al., 2012, Greig et al., 2013). A new theme of cortical patterning  
560 emerges, in which genetic factors intrinsically direct the spatial and temporal establishment  
561 of topographically organized axonal connections between the cortex and subcortical brain  
562 regions (Cadwell et al., 2019). Our initial hypothesis that cortical patterning genes, such as  
563 *Nr2f1*, known to modulate the size and positions of future cortical areas (O'Leary and Sahara,  
564 2008, Alfano and Studer, 2012, Cadwell et al., 2019), were good candidates to impart the  
565 spatial characteristics of corticopontine projections during development, was also supported  
566 by evidence of abnormal specification of layer V neurons upon loss of *Nr2f1*. For instance, we  
567 previously showed (i) abnormal temporal and spatial specification (Alfano et al., 2014,  
568 Armentano et al., 2007, Tomassy et al., 2010); (ii) altered intrinsic excitability and dendrite  
569 complexity (Del Pino et al., 2020) of layer V neurons in *Nr2f1* cortical mutants, and (iii)

570 behavioral defects in the execution of skilled voluntary movements but not locomotion of  
571 adult *Nr2f1* mutant mice (Tomassy et al., 2010). These previous observations prompted us to  
572 use *Nr2f1* genetic models as a paradigm to hypothesize the implication of cortical area  
573 mapping in corticopontine topography.

574

#### 575 **Mitotic versus postmitotic *Nr2f1* functions in layer V corticofugal projections**

576 Our previous data showed overall areal organization impairments in both *Nr2f1* mutant  
577 brains, independently of whether *Nr2f1* was inactivated in progenitors or postmitotic  
578 neurons. Then, gain-of-function experiments showed that area identity was most likely due  
579 to *Nr2f1* expression in postmitotic cells (Alfano et al., 2014). Here, we show for the first time  
580 that *Nr2f1* drives corticopontine connectivity differently in progenitors *versus* postmitotic  
581 neurons. While *Nr2f1* expressed by progenitor cells controls the ratio between corticopontine  
582 and corticospinal axonal projections, similarly to what happens in *C. elegans* with the ortholog  
583 UNC-55 (Zhou and Walthall, 1998, Petersen et al., 2011), postmitotic *Nr2f1* expression  
584 specifically acts on S1 topographic organization of corticopontine neurons (**Figure 8**). This  
585 suggests that early *Nr2f1* expression in progenitor cells is mainly required in the specification  
586 and axonal guidance of layer V subtypes, while later postmitotic expression is more implicated  
587 in the refinement of corticopontine topographical organization. Interestingly, the altered  
588 distribution of layer V YFP expression observed in the *Emx1*- and *Nex-cKO* cortex relative to  
589 control animals, correspond well with the differences in pontine innervation. A higher  
590 production of layer V neurons in S1 of *Emx1-cKO* mice leads to increased corticopontine  
591 innervation, in accordance with increased *Lmo4* expression, known to drive layer V neurons  
592 versus the pontine nuclei (Cederquist et al., 2013, Harb et al., 2016). Differently, the *Nex-cKO*  
593 S1 cortex maintains a similar number of YFP layer V neurons, but their axons project to  
594 pontine targets normally innervated by motor-derived cortical areas. Since only a  
595 subpopulation of layer V neurons express YFP in the S1 barrel field region, as previously  
596 reported (Porrero et al., 2010), fewer YFP projections arising from this region are labeled in  
597 pontine nuclei, but are nevertheless present, as demonstrated by corticopontine tracer  
598 injections from anterolateral cortical regions. Finally, increased signal expression in visual and  
599 auditory areas in the occipital cortex, corresponds with an increased innervation in



600 dorsolateral regions of pontine nuclei known to receive projections from the occipital cortex.  
601 This observation confirms our main conclusion that postmitotic Nr2f1 expression is involved  
602 in determining layer V corticopontine topographical mapping.

603

#### 604 **Revising the chrono-architectonic hypothesis of cortico-pontine circuit development**

605 Previous data in developing rats have shown that pontine neurons settle in the forming  
606 pontine nuclei in a shell-like fashion according to their birthdate with early born neurons  
607 forming the central core of the pontine nuclei and later born neurons consecutively settling  
608 around the earlier born neurons forming concentric rings (Altman and Bayer, 1987). In  
609 parallel, at early postnatal stages, corticopontine axons are chemotropically attracted as  
610 collateral branches from corticospinal axons (O'Leary and Terashima, 1988, Heffner et al.,  
611 1990), and innervate the pontine nuclei in a topographic inside-out pattern (Leergaard et al.,  
612 1995), which is further refined through adult stages (Leergaard and Bjaalie, 2007). Neurons in  
613 the frontal (motor) cortex project rostrally and medially in the pontine nuclei, neurons in the  
614 parietal (somatosensory) cortex project to central and caudal parts, neurons in the temporal  
615 (auditory) cortex to central and lateral regions, and neurons in the occipital (visual) cortex to  
616 lateral and rostral parts of the pontine nuclei (Leergaard and Bjaalie, 2007). This concentric  
617 organization of corticopontine projections suggests that the birthdate of pontine neurons and  
618 the inside-out genesis of the pontine nuclei is linked to the spatial organization of cortical  
619 inputs.

620 However, intrinsic differences in pontine neurons born at different times might also have an  
621 instructive role for corticopontine innervation. A recent study in mice showed that  
622 postmitotic expression of the HOX gene *Hoxa5* guides pontine neurons to settle caudally  
623 within the pontine nuclei, where they are targeted by projections from limb representations  
624 in the somatosensory cortex (Maheshwari et al., 2020). Moreover, ectopic *Hoxa5* expression  
625 in pontine neurons is sufficient to attract cortical somatosensory inputs, regardless of their  
626 spatial position in the pontine nuclei, showing that pontine neurons can play an instructive  
627 and attractive role in topographic input connectivity of corticopontine neurons (Maheshwari  
628 et al., 2020).

629 Nevertheless, maturational gradients in the pontine nuclei cannot fully explain the complexity  
630 of the fine-grained somatotopic topographic connectivity pattern between cortical input and  
631 pontine neuron targets. Since the establishment of topographic maps requires multiple  
632 processes and structures, it is conceivable that the position and specific intrinsic molecular  
633 programs of both presynaptic afferents and postsynaptic target neurons contribute to this  
634 complex corticopontine connectivity map. Indeed, our data show that without affecting the  
635 development and maturation of pontine neurons, corticopontine Nr2f1-deficient layer V  
636 axons originating from S1 areas in the parietal cortex will abnormally target the pontine  
637 region normally deputed to corticopontine motor axons. By contrast, Nr2f1-deficient axons  
638 originating from the frontal and medial cortex will innervate the expected pontine region  
639 allocated to motor axons (**Figure 8**). This strongly suggests that during the establishment of  
640 corticopontine topography, both structures, the neocortex and the pons need to be properly  
641 pre-patterned by factors involved in spatial and temporal control of neurogenesis, such as  
642 Nr2f1 for the cortex, and Hoxa5 for the pontine nuclei.

643

#### 644 **Conclusion and outlook**

645 With the present study, we have provided new insights into the developmental mechanisms  
646 establishing topographical organization by showing that gradient cortical expressions of  
647 transcription factors, in this case Nr2f1, are directly involved in the establishment of  
648 corticopontine topographic mapping. However, it is likely that other factors regulating area  
649 size and positions might also be implicated in the same process. We conclude that distinct  
650 molecular mechanisms in the source (cerebral cortex) and target (pontine nuclei) regions  
651 must be coordinated during the establishment of corticopontine topography. Identifying the  
652 molecular pathways within the cortex and pontine nuclei, as well as the mechanisms and  
653 molecules governing their interaction remains an open question for further studies.

654

655

656

## 657 **STAR Methods**

### 658 **Topographical map of corticopontine projections from somatosensory and motor areas**

659 To establish a 3D benchmark map of corticopontine projections from somatosensory and  
660 motor areas in adult wild type mice, we utilized a selection of public experimental tract-  
661 tracing data available from the Allen Institute mouse brain connectivity atlas  
662 (<http://connectivity.brain-map.org/>). We selected 11 experiments in which the anterograde  
663 tracer EGFP was injected in the right primary/secondary motor cortex (n =6) or primary  
664 somatosensory cortex (n = 5) of wild type C57BL/6J mice (**Supplementary Table 1**). Serial two  
665 photon fluorescence images were interactively inspected online using the Projection High  
666 Resolution Image viewer of the Allen Institute, and from each case, 5 sagittal oriented images  
667 of the right pontine nuclei (matching the orientation of the histological material generated  
668 from our knock-out mice), spaced at ~100  $\mu\text{m}$  were captured by screen shot from the largest  
669 3D multiplane thumbnail viewer. The resolution of the captured images was up-sampled  
670 three times original size before their spatial alignment to the CCFv3 was optimized using the  
671 tools QuickNII (Puchades et al., 2019) and VisuAlign (RRID), as described below. These images  
672 were used to create 3D representations of the axonal labeling in the pontine nuclei (**Figure 2**;  
673 see below).

### 674 **Animals**

675 All mice used were bred in a C57BL/6J background. Male and female animals at any stage of  
676 development were used. All experiments were conducted in accordance with the French  
677 Animal Welfare Act and European guidelines for the use of experimental animals, using  
678 protocols approved by the French Ministry of Education, Research and Innovation and the  
679 local ethics committee (CIEPAL NCE/2019–548, Nice) under authorization #15 349 and #15  
680 350. *Nr2f1/COUP-TF<sup>fl/fl</sup>* mice were crossed with *Emx1-Cre-recombinase* mice to inactivate  
681 *Nr2f1/COUP-TF* exclusively in cortical progenitors and their progeny (Armentano et al., 2007)  
682 or with *Nex-Cre-recombinase* mice to abolish *Nr2f1/COUP-TF* expression from postmitotic  
683 neurons (Alfano et al., 2014). Littermate *Nr2f1/COUP-TF<sup>fl/fl</sup>* mice without the presence of the  
684 *Cre-recombinase* gene (*Cre-negatives*) were considered controls (**Supplementary Table 2**).  
685 For postnatal (P)21 and adult topographic map analysis, *Emx1-cKO* and *Nex-cKO* animals were

686 further crossed with *Thy1-eYFP-H* mice to specifically label layer V projection neurons, as  
687 previously reported (Harb et al., 2016, Porrero et al., 2010). Mice were genotyped as  
688 previously described (Alfano et al., 2014, Armentano et al., 2007, Harb et al., 2016). Control  
689 and mutant littermates were genotyped as *Nr2f1<sup>fl/fl</sup>:Thy1-eYFP-H<sup>T/+</sup>* and *Nr2f1<sup>fl/fl</sup>:Emx1-  
690 Cre:Thy1-eYFP-H<sup>T/+</sup>* or *Nr2f1<sup>fl/fl</sup>:Nex-Cre:Thy1-eYFP-H<sup>T/+</sup>*, respectively. For simplicity, mutant  
691 mice are named *Emx1-cKO* and *Nex-cKO* throughout the text. Midday of the day of the  
692 observed vaginal plug was considered as embryonic day 0.5 (E0.5).

### 693 **Anterograde tracing of corticospinal axons in early postnatal mice**

694 P4-P5 animals were anesthetized on ice for 5 min and kept on ice during the whole procedure.  
695 Viral particles were produced from the AAV9-CAGtdTomato plasmid by the Alexis Bemelmans  
696 (CEA, France) Company, and diluted 1:50 in TE-Buffer (Qiagen, #1018499) to a final  
697 concentration of 1.75e12 vg/ml (kindly donated by I. Dusart, Pierre and Marie Curie  
698 University, Paris, France). Approximately 0.5/1ul was injected unilaterally in different rostral-  
699 caudal and medio-lateral brain locations of control and *Nex-cKO* pups, as previously described  
700 in (Gu et al. 2017).

### 701 **Microscopic imaging**

702 Mosaic microscopic images were acquired using an Axio Imager M2 epifluorescence  
703 microscope (Carl Zeiss Microscopy GmbH, Jena, Germany) equipped with a halogen lamp, a  
704 MCU 2008 motorized stage, and an EC Plan-Neofluar 10x/0.30 and an AxioCam MRm camera.  
705 ZEN blue software was used for imaging and automatic stitching. Images were exported in  
706 TIFF format and serially ordered from lateral to medial, rotated and if needed, mirrored to  
707 consistent anatomical orientation using Adobe Photoshop CS6 (RRID: SCR\_014199), before  
708 being converted to PNG format and resized to 60% of original size using ImageJ  
709 (RRID:SCR\_003070) with bilinear interpolation. The resized serial images were loaded into  
710 Adobe Photoshop as a stack, spatially aligned using the ventral surfaces of the pons and  
711 cerebral peduncle as landmarks, cropped and exported as individual PNG files.

712 For comparative analyses of topographical organization (see below), variations in YFP signal  
713 expression intensity within and between groups were normalized by adjusting the brightness

714 and contrast of images to equal levels using a custom-made histogram matching script  
715 available for ImageJ (National Institutes of Health; <https://imagej.nih.gov/>). One selected,  
716 representative case (Experiment 5, Cre-negative, nr: 14250, **Supplementary Table 2**) was  
717 used as reference.

### 718 **Spatial alignment to common 3D reference atlas**

719 Serial sectional images were spatially registered to the *Allen Mouse Common Coordinate*  
720 *Framework*, version 3, 2017 edition of the delineations (CCFv3, (Wang et al., 2020) using the  
721 QuickNII software tool (RRID:SCR\_016854; (Puchades et al., 2019). Multiple anatomical  
722 landmarks (hippocampus, caudoputamen, inferior and superior colliculus, and external  
723 surface of the neocortex) were used to determine the mediolateral position and orientation  
724 of the sagittal section images. For each section image, custom atlas diagrams were aligned to  
725 anatomical landmarks in the experimental images using affine transformations, with  
726 emphasis on matching the ventral surface of the pons and white matter tracts close to the  
727 pontine nuclei and exported as PNG images. To co-display images and the spatially registered  
728 custom atlas images, we used the software tool LocaliZoom, which is embedded in the  
729 Navigator3 image management system ([bit.ly/navigator3](http://bit.ly/navigator3)), developed and hosted by the  
730 Neural Systems Laboratory at the University of Oslo, Norway.

### 731 **Cortical distribution analysis in *Emx1-cKO* and *Nex-cKO* mutants**

732 Serial section images from *Nex-cKO* and *Emx1-cKO* mutants co-registered to the *Allen Mouse*  
733 *Brain Connectivity Atlas* were semi-quantitatively analyzed using a 5-stage scoring table based  
734 on relative density of cells in the cortical mantle (**Figure 4A-D'**). Each brain region was scored  
735 from 0 (absent signal) to 4 (very high signal), characterized by high number of cells, dense and  
736 extensive overlap and intense signal intensity (**Figure 4E**). The quantifications were  
737 summarized graphically and displayed as histograms (**Figure 4F**).

### 738 **Corticospinal tract morphometric analysis in *Emx1-cKO* and *Nex-cKO* mutants**

739 Serial section images from *Nex-cKO* and *Emx1-cKO* mutants were analyzed by using the *Fiji-*  
740 *ImageJ Software* tool (Schindelin et al., 2015) used to determine the total dorsoventral width  
741 of the bundle expressing fluorescent signal in the descending fiber tract in different positions:

742 rostrally and caudally to the pontine nuclei, and 250  $\mu\text{m}$  and 500  $\mu\text{m}$  caudal to the nuclei. The  
743 width of separate fiber fascicles was also measured 250  $\mu\text{m}$  and 500 $\mu\text{m}$  from the terminal  
744 edge of the pontine nuclei (**Figure 5A'**).

#### 745 **Analysis of tracer injection sites**

746 Serial section images of cortical tracer injections in *Nex-cKO* brains (**Supplementary Table 3**)  
747 and experiments taken from the *Allen Mouse Brain Connectivity Atlas*, were spatially aligned  
748 using QuickNII and VisuAlign, as described above. The center positions of the injection sites  
749 were annotated as a point-coordinate using LocaliZoom, co-displayed with the CCFv3 atlas in  
750 the 3D viewer tool MeshView (RRID:SCR\_017222). The mouse brain atlas of Franklin and  
751 Paxinos (Franklin and Paxinos, 2008) was used to aid the interpretation of injection site  
752 locations. This visualization was used to select spatially corresponding injection site locations  
753 for analyses of spatial distribution of corticopontine projections.

#### 754 **Histology, immunohistochemistry and *in situ* hybridization**

755 At age P8, P21 and adulthood, animals were anesthetized by intraperitoneal injection of a  
756 mixture of Tiletamine-Zolazepam-Xylazine-Buprenorphine and intracardially perfused with PB  
757 Saline (PBS) followed by 4% paraformaldehyde (PFA) in PBS. Volumes were 15, 20 and 30 ml,  
758 respectively. Brains were removed from the skull and postfixed for 4 h at 4°C in 4% PFA, before  
759 being vibratome-sectioned in 100 $\mu\text{m}$  (adult samples) or 150 $\mu\text{m}$  (P8 and P21 samples) thick  
760 sagittal sections. All sections were incubated overnight at 4°C in a solution of 0.5% Triton X-  
761 100, 3% BSA, 10% goat serum in PBS, for permeabilization and reduction of non-specific  
762 binding of antibodies. For immunofluorescence (IF), sections were incubated for 2 days at 4°C  
763 with primary antibodies in a solution of 0.5% Triton X-100, 10% goat serum in PBS, and then  
764 overnight at 4°C with relative secondary antibodies and HOECHST diluted in PBS. For the  
765 complete list of primary and secondary antibodies, see **Supplementary Table 5**. Sections were  
766 washed several times in PBS, then transferred on Superfrost plus slides (ThermoScientific),  
767 covered and dried for 30 min to 1 h, and finally mounted with the Mowiol (Sigma-Aldrich)  
768 mounting medium. Whole mount *in situ* hybridization of *Nr2f1* mRNA on P7 brains was  
769 performed according to previously published protocols (Mercurio et al., 2019).

## 770 **Semi-quantitative recording and 3D visualization of spatial distribution patterns**

771 To investigate and compare the 3D distributions of YFP signal expression or anterograde  
772 axonal labelling within the pontine nuclei, we used the annotation functionality in the  
773 LocaliZoom tool to semi-quantitatively record YFP signal expression or labelled axons in all  
774 sections through the pontine nuclei as point coordinates (specified in the coordinate system  
775 of the reference atlas, CCFv3), reflecting the overall density of signal/labelling observed in the  
776 images (**Figure 2B,C,G,H**). To compensate for the spacing between sections and allow  
777 inspection of point distributions perpendicularly to the section angle, the z-coordinate of each  
778 point was randomly displaced within the thickness of the gap between sections using a  
779 custom Python script. The point-coordinates were co-displayed in the MeshView 3D viewer  
780 tool (**Figures 2, 3, 6, 7**).

## 781 **Data and Code Availability**

782 All microscopic images and derived 3D point coordinate data representing the YFP signal  
783 expression or axonal labelling in the pontine nuclei generated in this project will be shared via  
784 the EBRAINS research infrastructure (<https://search.kg.ebrains.eu/>) as high-resolution TIFF  
785 images, together with customized, spatially matching reference atlas plates in PNG format.  
786 The custom Python script (spread.py) used to randomly displace data points within the  
787 thickness of a section is available upon request. The LocaliZoom and Meshview viewer tools  
788 are available from <https://search.kg.ebrains.eu/>

## 789 **ACKNOWLEDGEMENTS**

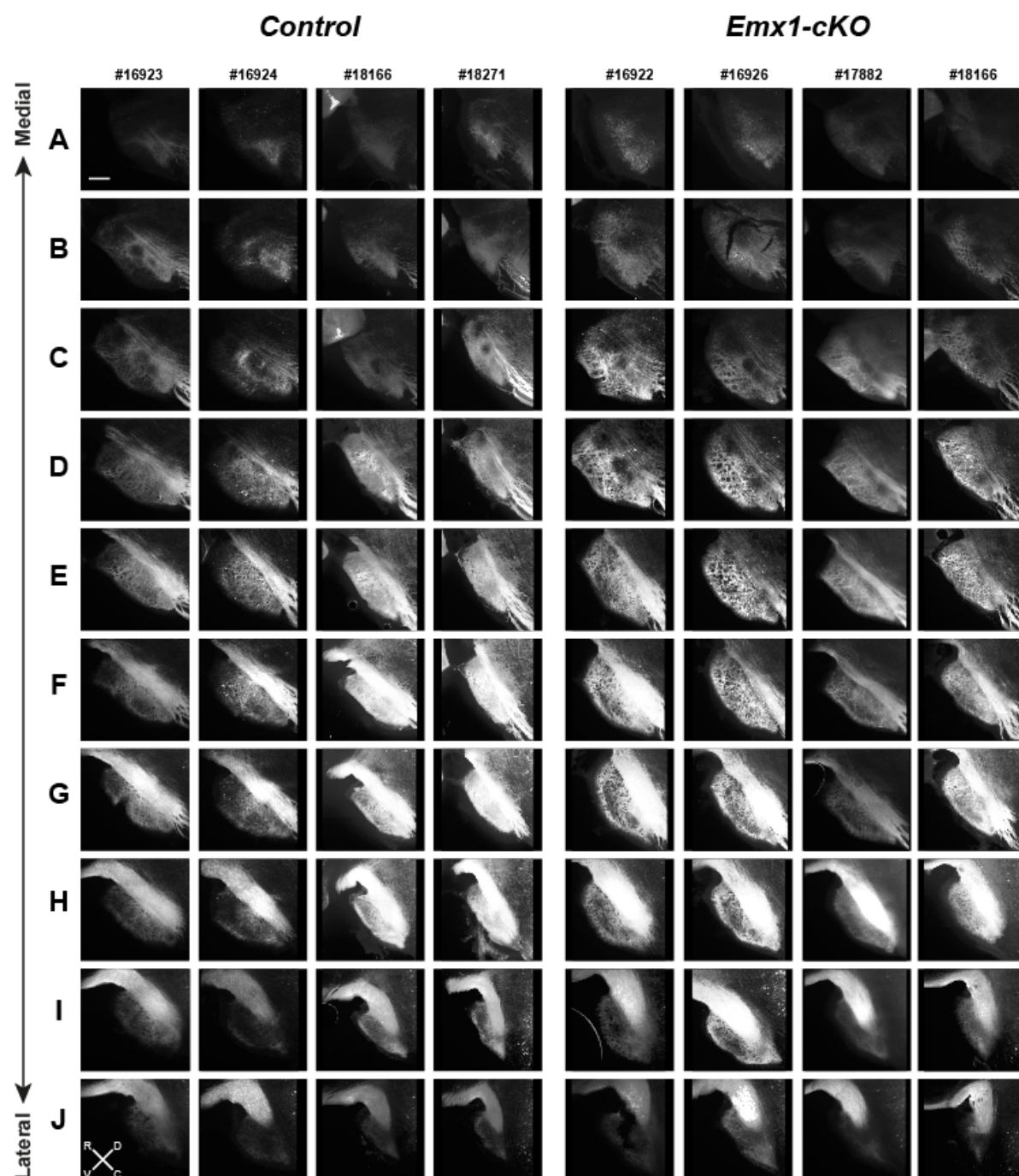
790 We thank Isabelle Dusart in Paris for providing us with AAV9-CAG-tdTomato viral particles  
791 produced by Alexis Bemelmans (CEA, France), Sara Mercurio and Silvia Nicolis for the Nr2f1  
792 stained whole-mount brain, Nicolaas Groeneboom and Gergely Csucs for expert technical  
793 assistance, the iBV PRISM platform for imaging support, and Sharon Yates, and Maja A.  
794 Puchades for useful discussions. This work was funded by the “Fondation Recherche  
795 Médicale; Equipe FRM 2015” #DEQ20150331750 to M.S.; by an “Investments for the Future”  
796 LabEx SIGNALIFE (grant ANR-11- LABX-0028-01) to M.S., by a PhD contract from Région  
797 PACA/Inserm and FRM 4<sup>th</sup> year PhD for C.T, with additional funding from the European

798 Union's Horizon 2020 Framework Program for Research and Innovation under the Specific  
799 Grant Agreement No. 785907 (Human Brain Project SGA2), Specific Grant Agreement No.  
800 945539 (Human Brain Project SGA3), and The Research Council of Norway under Grant  
801 Agreement No. 269774 (INCF Norwegian Node) to JGB and TBL.

802 **Competing interests:** The authors declare no financial and non-financial competing interests.  
803

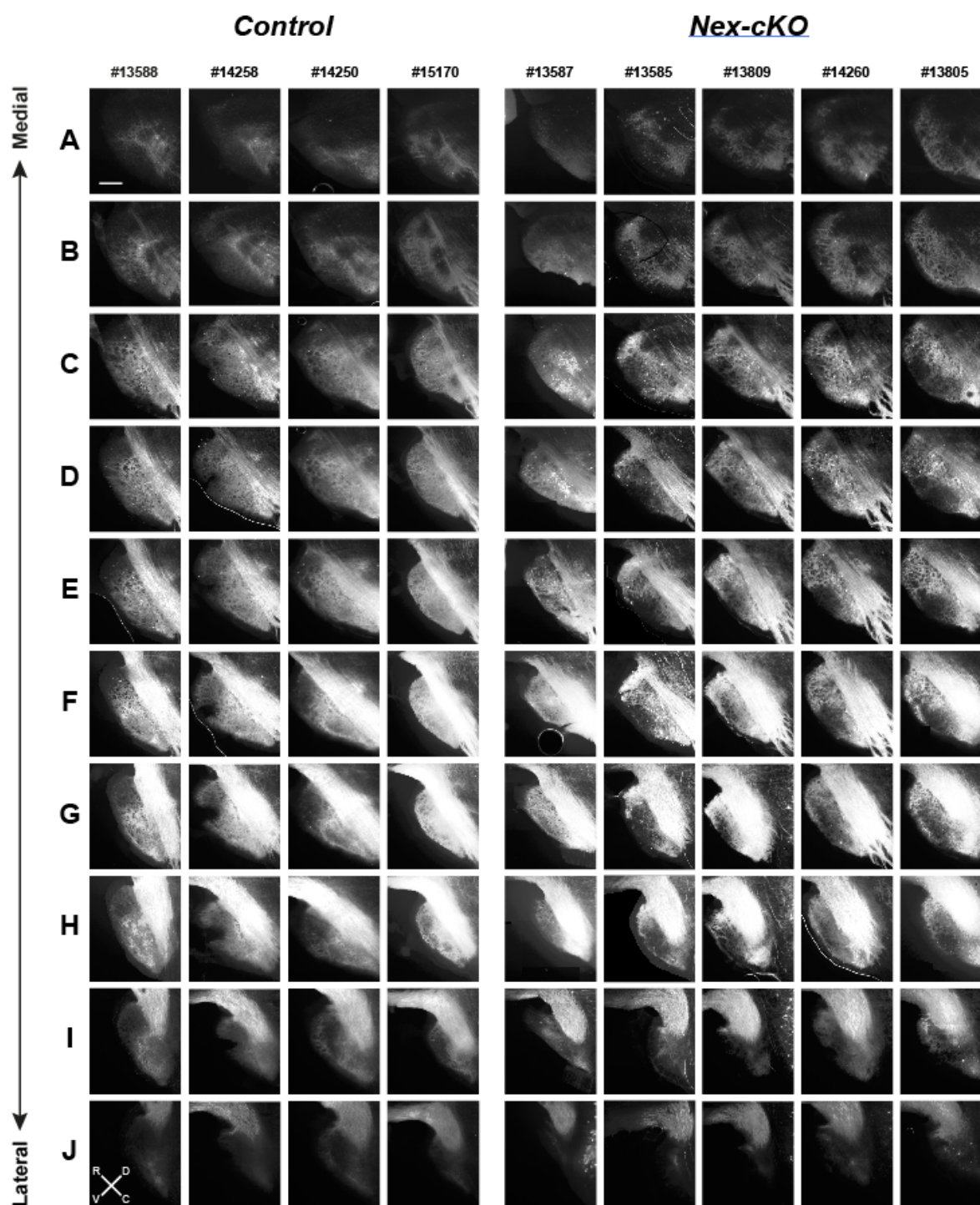


804 SUPPLEMENTARY FIGURES



805  
806  
807  
808  
809  
810  
811  
812

**Supplementary Figure 1.** Fluorescence microscopy images of the pontine nuclei in sagittal sections from 4 control- and 4 *Emx1*-cKO mice. Columns show images from one animal, with sections from corresponding levels from medial to lateral are sorted from top to bottom (rows A-J). The intensity levels of the images have been normalized. Signal expression in *Emx1*-cKO mice is more widespread and more diffusely distributed in the pontine nuclei, relative to controls. Scale bar, 200  $\mu$ m.



813  
814

815 **Supplementary Figure 2.** Fluorescence microscopy images of the pontine nuclei in sagittal sections  
816 from 4 control- and 4 Nex-cKO mice. Columns show images from one animal, with sections from  
817 corresponding levels from medial to lateral are sorted from top to bottom (rows A-J). The intensity  
818 levels of the images have been normalized. Signal expression in Nex-cKO mice is more clearly reduced  
819 or absent in the central core region of the pontine nuclei, relative to controls. Scale bar, 200  $\mu$ m.  
820

821 **SUPPLEMENTARY TABLES**

822 **Supplementary Table 1**

<b>Allen Mouse Brain Connectivity database</b>					
<b>Experiment number #</b>	<b>Sex</b>	<b>Age (<math>\pm 2</math>)</b>	<b>Genotype</b>	<b>Injection site</b>	<b>Shown in</b>
100141780	Male	P56	C57BL/6J	Primary motor cortex	Fig. 3, 7B and 7K
114290938	male	P56	C57BL/6J	Primary somatosensory cortex, mouth region	Fig. 2A, 2B, 3, 7B and 7J
112229814	male	P56	C57BL/6J	Primary somatosensory cortex, upper limb region	Fig. 3, 7B and 7F
112952510	male	P56	C57BL/6J	Secondary motor cortex	Fig. 3
114292355	male	P56	C57BL/6J	Primary somatosensory cortex, lower limb region	Fig. 3, 7B and 7F
126908007	male	P56	C57BL/6J	Primary somatosensory cortex, nose region	Fig. 3, 7B and 7I
127084296	male	P56	C57BL/6J	Secondary motor cortex	Fig. 3
127866392	male	P56	C57BL/6J	Primary somatosensory cortex, barrel field region	Fig. 3
141602484	male	P56	C57BL/6J	Secondary motor cortex	Fig. 3
141603190	male	P56	C57BL/6J	Secondary motor cortex	Fig. 3
585025284	male	P56	C57BL/6J	Secondary motor cortex	Fig. 3

823

824 **Supplementary Table 2**

Adult					
Exp. #	Animal #	Sex	Age	Genotype	Shown in
1	13588	female	P33	<i>Thy1-eYFP<sup>T/+</sup>; Nr2f1<sup>fl/fl</sup></i>	Fig. 4, 5, 6 and Suppl. Fig.1, 2
1	13587	female	P33	<i>Thy1-eYFP<sup>T/+</sup>; Nr2f1<sup>fl/fl</sup>; Nex-Cre</i>	Fig. 4, 5, 6 and Suppl. Fig.1, 2
2	13585	male	P62	<i>Thy1-eYFP<sup>T/+</sup>; Nr2f1<sup>fl/fl</sup>; Nex-Cre</i>	Fig. 4, 5, 6 and Suppl. Fig.1, 2
3	13809	male	P57	<i>Thy1-eYFP<sup>T/+</sup>; Nr2f1<sup>fl/fl</sup>; Nex-Cre</i>	Fig. 4, 5, 6 and Suppl. Fig.1, 2
4	14258	male	P57	<i>Thy1-eYFP<sup>T/+</sup>; Nr2f1<sup>fl/fl</sup></i>	Fig. 4, 5, 6 and Suppl. Fig.1, 2
4	14260	male	P57	<i>Thy1-eYFP<sup>T/+</sup>; Nr2f1<sup>fl/fl</sup>; Nex-Cre</i>	Fig. 4, 5, 6 and Suppl. Fig.1, 2
5	13805	male	P55	<i>Thy1-eYFP<sup>T/+</sup>; Nr2f1<sup>fl/fl</sup>; Nex-Cre</i>	Fig. 4, 5, 6 and Suppl. Fig.1, 2
5	14250	male	P72	<i>Thy1-eYFP<sup>T/+</sup>; Nr2f1<sup>fl/fl</sup></i>	Fig. 4, 5, 6 and Suppl. Fig.1, 2
5	15170	male	P75	<i>Thy1-eYFP<sup>T/+</sup>; Nr2f1<sup>fl/fl</sup></i>	Fig. 4, 5, 6 and Suppl. Fig.1, 2
6	16922	male	P76	<i>Thy1-eYFP<sup>T/+</sup>; Nr2f1<sup>fl/fl</sup>; Emx1-Cre</i>	Fig. 4, 5, 6 and Suppl. Fig.1, 2
6	16923	male	P76	<i>Thy1-eYFP<sup>T/+</sup>; Nr2f1<sup>fl/fl</sup></i>	Fig. 4, 5, 6 and Suppl. Fig.1, 2
6	16924	male	P76	<i>Thy1-eYFP<sup>T/+</sup>; Nr2f1<sup>fl/fl</sup></i>	Fig. 4, 5, 6 and Suppl. Fig.1, 2
6	16926	male	P76	<i>Thy1-eYFP<sup>T/+</sup>; Nr2f1<sup>fl/fl</sup>; Emx1-Cre</i>	Fig. 4, 5, 6 and Suppl. Fig.1, 2
7	17882	male	P72	<i>Thy1-eYFP<sup>T/+</sup>; Nr2f1<sup>fl/fl</sup>; Emx1-Cre</i>	Fig. 4, 5, 6 and Suppl. Fig.1, 2
8	18046	female	P109	<i>Thy1-eYFP<sup>T/+</sup>; Nr2f1<sup>fl/fl</sup>; Emx1-Cre</i>	Fig. 4, 5, 6 and Suppl. Fig.1, 2
8	18166	female	P98	<i>Thy1-eYFP<sup>T/+</sup>; Nr2f1<sup>fl/fl</sup></i>	Fig. 4, 5, 6 and Suppl. Fig.1, 2
8	18271	female	P87	<i>Thy1-eYFP<sup>T/+</sup>; Nr2f1<sup>fl/fl</sup></i>	Fig. 4, 5, 6 and Suppl. Fig.1, 2
9	19606	female	P86	<i>Thy1-eYFP<sup>T/+</sup>; Nr2f1<sup>fl/fl</sup>; Emx1-Cre</i>	Fig. 5
9	19607	female	P86	<i>Thy1-eYFP<sup>T/+</sup>; Nr2f1<sup>fl/fl</sup>; Emx1-Cre</i>	Fig. 5

825

826 **Supplementary Table 3**

<b>P21 – unilateral CST tracing</b>			
<b><i>Tracer injected in motor cortex</i></b>			
<b>Experiment #</b>	<b>Animal #</b>	<b>Genotype</b>	<b>Shown in</b>
2	11643_13	<i>Ctrl</i>	Fig. 7B and 7C
2	11643_16	<i>Nex-cKO</i>	Not shown
2	11643_17	<i>Nex-cKO</i>	Fig. 7B and 7E
2	11796_2	<i>Ctrl</i>	Not shown
2	11796_8	<i>Ctrl</i>	Not shown
2	11796_9	<i>Ctrl</i>	Not shown
3	18035_1	<i>Ctrl</i>	Fig. 7B and 7E
3	18035_2	<i>Ctrl</i>	Fig. 7B and 7D
3	18035_7	<i>Ctrl</i>	Not shown
3	18035_3	<i>Nex-cKO</i>	Fig. 7B and 7D
3	18035_4	<i>Nex-cKO</i>	Not shown
3	18035_8	<i>Nex-cKO</i>	Fig. 7B and 7C
4	19423_2	<i>Ctrl</i>	Not shown
4	19423_3	<i>Ctrl</i>	Not shown
4	19423_4	<i>Nex-cKO</i>	Not shown
4	19423_5	<i>Nex-cKO</i>	Not shown
<b><i>Tracer injected in somatosensory cortex</i></b>			
4	19423_6	<i>Nex-cKO</i>	Fig. 7B and 7F
4	19423_7	<i>Nex-cKO</i>	Fig. 7B and 7G
6	11431_1	<i>Nex-cKO</i>	Fig. 7B and 7I
6	11431_3	<i>Nex-cKO</i>	Fig. 7B and 7H
6	11431_4	<i>Nex-cKO</i>	Fig. 7B and 7K
6	11431_6	<i>Ctrl</i>	Fig. 7B and 7H
6	11431_7	<i>Nex-cKO</i>	Fig. 2F, 2G, 7B and 7J

827  
828  
829

830 **Supplementary Table 4:**  
831

**Figure 4 – Cortical distribution of YFP-H positive cells**

Area	Hypothesis	Mean 1	Mean 2	Mean diff.	95,00% CI of diff	Summary	Adjusted P.
PFC	Ctrl vs. Nex-cKO	1.172	0.3174	0.8543	-0.209 to 1.918	ns	0.3142
	Ctrl vs. Emx1-cKO	1.172	0.9523	0.2194	-0.8439 to 1.283	ns	>0.9999
	Nex-cKO vs. Emx1-cKO	0.3174	0.9523	-0.6349	-1.8 to 0.5299	ns	>0.9999
ACC	Ctrl vs. Nex-cKO	2.411	1.104	1.307	0.2434 to 2.37	**	0.0042
	Ctrl vs. Emx1-cKO	2.411	1.411	1	-0.06316 to 2.063	ns	0.0897
	Nex-cKO vs. Emx1-cKO	1.104	1.411	-0.3065	-1.471 to 0.8583	ns	>0.9999
GC	Ctrl vs. Nex-cKO	0.5317	0.09524	0.4365	-0.7283 to 1.601	****	<0.0001
	Ctrl vs. Emx1-cKO	0.5317	0.09524	0.4365	-0.7283 to 1.601	ns	0.1008
	Nex-cKO vs. Emx1-cKO	0.09524	0.09524	0	-1.345 to 1.345	***	0.0001
M2	Ctrl vs. Nex-cKO	1.515	2.773	1.515	1.709 to 3.836	****	<0.0001
	Ctrl vs. Emx1-cKO	3.301	0.9872	3.301	-0.07613 to 2.051	ns	>0.9999
	Nex-cKO vs. Emx1-cKO	3.301	-1.785	3.301	-2.95 to -0.6207	****	<0.0001
M1	Ctrl vs. Nex-cKO	4.217	1.818	2.399	1.336 to 3.462	ns	>0.9999
	Ctrl vs. Emx1-cKO	4.217	3.703	0.5139	-0.5495 to 1.577	**	0.0016
	Nex-cKO vs. Emx1-cKO	1.818	3.703	-1.885	-3.05 to -0.7202	****	<0.0001
S1	Ctrl vs. Nex-cKO	3.346	2.922	0.4237	-0.6396 to 1.487	ns	>0.9999
	Ctrl vs. Emx1-cKO	3.346	4.74	-1.394	-2.458 to -0.331	**	0.0016
	Nex-cKO vs. Emx1-cKO	2.922	4.74	-1.818	-2.983 to -0.6533	****	<0.0001
A	Ctrl vs. Nex-cKO	0.8868	1.803	-0.9158	-1.979 to 0.1475	ns	0.1883
	Ctrl vs. Emx1-cKO	0.8868	3.66	-2.773	-3.836 to -1.71	****	<0.0001
	Nex-cKO vs. Emx1-cKO	1.803	3.66	-1.857	-3.022 to -0.6922	****	<0.0001
V	Ctrl vs. Nex-cKO	0.9544	2.686	-1.732	-2.795 to -0.6684	****	<0.0001
	Ctrl vs. Emx1-cKO	0.9544	4.045	-3.091	-4.154 to -2.027	****	<0.0001
	Nex-cKO vs. Emx1-cKO	2.686	4.045	-1.359	-2.524 to -0.1942	**	0.0086
RSC	Ctrl vs. Nex-cKO	0.8826	2.101	-1.219	-2.282 to -0.1553	*	0.0108
	Ctrl vs. Emx1-cKO	0.8826	3.024	-2.142	-3.205 to -1.078	****	<0.0001
	Nex-cKO vs. Emx1-cKO	2.101	3.024	-0.923	-2.088 to 0.2418	ns	0.3454

**Figure 5E – Rostral LFP diameter**

Section	Hypothesis	Mean 1	Mean 2	Mean diff.	95,00% CI of diff	Summary	Adjusted P.
1	Ctrl vs. Nex-cKO	0	0	0	-116.9 to 116.9	ns	>0.9999
	Ctrl vs. Emx1-cKO	0	0	0	-116.9 to 116.9	ns	>0.9999
	Nex-cKO vs. Emx1-cKO	0	0	0	-124.9 to 124.9	ns	>0.9999
2	Ctrl vs. Nex-cKO	0	28.29	-28.29	-145.2 to 88.57	ns	0.836
	Ctrl vs. Emx1-cKO	0	0	0	-116.9 to 116.9	ns	>0.9999
	Nex-cKO vs. Emx1-cKO	28.29	0	28.29	-96.64 to 153.2	ns	0.8549
3	Ctrl vs. Nex-cKO	0	132.7	-132.7	-249.6 to -15.84	*	0.0215
	Ctrl vs. Emx1-cKO	0	0	0	-116.9 to 116.9	ns	>0.9999
	Nex-cKO vs. Emx1-cKO	132.7	0	132.7	7.775 to 257.6	*	0.0343
4	Ctrl vs. Nex-cKO	0	179.6	-179.6	-296.5 to -62.77	**	0.001
	Ctrl vs. Emx1-cKO	0	0	0	-116.9 to 116.9	ns	>0.9999
	Nex-cKO vs. Emx1-cKO	179.6	0	179.6	54.71 to 304.6	**	0.0023
5	Ctrl vs. Nex-cKO	0	175.9	-175.9	-292.8 to -59.04	**	0.0013
	Ctrl vs. Emx1-cKO	0	55.34	-55.34	-172.2 to 61.52	ns	0.5052
	Nex-cKO vs. Emx1-cKO	175.9	55.34	120.6	-4.369 to 245.5	ns	0.0612
6	Ctrl vs. Nex-cKO	24.35	169.6	-145.2	-262.1 to -28.37	*	0.0103
	Ctrl vs. Emx1-cKO	24.35	115	-90.67	-207.5 to 26.2	ns	0.1624
	Nex-cKO vs. Emx1-cKO	169.6	115	54.57	-70.37 to 179.5	ns	0.5592
7	Ctrl vs. Nex-cKO	117	231.4	-114.4	-231.3 to 2.467	ns	0.0565
	Ctrl vs. Emx1-cKO	117	234.6	-117.7	-234.5 to -0.8201	*	0.048
	Nex-cKO vs. Emx1-cKO	231.4	234.6	-3.287	-128.2 to 121.6	ns	0.9979
8	Ctrl vs. Nex-cKO	241.7	187.5	54.13	-66.26 to 174.5	ns	0.5401
	Ctrl vs. Emx1-cKO	241.7	293	-51.33	-171.7 to 69.06	ns	0.5746
	Nex-cKO vs. Emx1-cKO	187.5	293	-105.5	-230.4 to 19.47	ns	0.1168
9	Ctrl vs. Nex-cKO	316.6	267.9	48.71	-68.15 to 165.6	ns	0.5888
	Ctrl vs. Emx1-cKO	316.6	250.1	66.55	-56.81 to 189.9	ns	0.4128
	Nex-cKO vs. Emx1-cKO	267.9	250.1	17.83	-113.2 to 148.9	ns	0.9449
10	Ctrl vs. Nex-cKO	318.9	194.4	124.6	7.715 to 241.4	*	0.0335
	Ctrl vs. Emx1-cKO	318.9	205.8	113.1	-3.738 to 230	ns	0.0602
	Nex-cKO vs. Emx1-cKO	194.4	205.8	-11.45	-136.4 to 113.5	ns	0.9746
11	Ctrl vs. Nex-cKO	231.1	88.06	143.1	-163 to 449.1	ns	0.514
	Ctrl vs. Emx1-cKO	231.1	64.04	167.1	-82.79 to 416.9	ns	0.258
	Nex-cKO vs. Emx1-cKO	88.06	64.04	24.02	-225.8 to 273.9	ns	0.9721

12	Ctrl vs. Nex-cKO	276.1	179.6	96.5	-26.86 to 219.9	ns	0.1576
	Ctrl vs. Emx1-cKO	276.1	136.5	139.6	16.23 to 263	*	0.022
	Nex-cKO vs. Emx1-cKO	179.6	136.5	43.09	-93.77 to 179.9	ns	0.7389
13	Ctrl vs. Nex-cKO	201.9	180.5	21.33	-243.7 to 286.3	ns	0.9804
	Ctrl vs. Emx1-cKO	201.9	44.45	157.4	-40.14 to 354.9	ns	0.1471
	Nex-cKO vs. Emx1-cKO	180.5	44.45	136.1	-113.8 to 385.9	ns	0.4059
14	Ctrl vs. Nex-cKO	218.4	114.6	103.8	-19.52 to 227.2	ns	0.1182
	Ctrl vs. Emx1-cKO	218.4	95.41	123	-0.3344 to 246.4	ns	0.0508
	Nex-cKO vs. Emx1-cKO	114.6	95.41	19.19	-117.7 to 156	ns	0.9416
15	Ctrl vs. Nex-cKO	154.7	59.11	95.61	-21.25 to 212.5	ns	0.1328
	Ctrl vs. Emx1-cKO	154.7	51.17	103.6	-13.31 to 220.4	ns	0.0942
	Nex-cKO vs. Emx1-cKO	59.11	51.17	7.94	-117 to 132.9	ns	0.9877
16	Ctrl vs. Nex-cKO	101.6	16.85	84.78	-32.09 to 201.6	ns	0.2035
	Ctrl vs. Emx1-cKO	101.6	18.75	82.87	-33.99 to 199.7	ns	0.2183
	Nex-cKO vs. Emx1-cKO	16.85	18.75	-1.908	-126.8 to 123	ns	0.9993
17	Ctrl vs. Nex-cKO	60.94	0	60.94	-55.93 to 177.8	ns	0.4374
	Ctrl vs. Emx1-cKO	60.94	0	60.94	-55.93 to 177.8	ns	0.4374
	Nex-cKO vs. Emx1-cKO	0	0	0	-124.9 to 124.9	ns	>0.9999
18	Ctrl vs. Nex-cKO	28.85	0	28.85	-88.02 to 145.7	ns	0.8301
	Ctrl vs. Emx1-cKO	28.85	0	28.85	-88.02 to 145.7	ns	0.8301
	Nex-cKO vs. Emx1-cKO	0	0	0	-124.9 to 124.9	ns	>0.9999
19	Ctrl vs. Nex-cKO	0	0	0	-112 to 112	ns	>0.9999
	Ctrl vs. Emx1-cKO	0	0	0	-116.9 to 116.9	ns	>0.9999
	Nex-cKO vs. Emx1-cKO	0	0	0	-120.4 to 120.4	ns	>0.9999

**Figure 5F – Caudal LFP diameter**

Section	Hypothesis	Mean 1	Mean 2	Mean diff.	95,00% CI of diff	Summary	Adjusted P.
1	Ctrl vs. Nex-cKO	0	0	0	-88.51 to 88.51	ns	>0.9999
	Ctrl vs. Emx1-cKO	0	0	0	-88.51 to 88.51	ns	>0.9999
	Nex-cKO vs. Emx1-cKO	0	0	0	-94.62 to 94.62	ns	>0.9999
2	Ctrl vs. Nex-cKO	0	46.89	-46.89	-135.4 to 41.62	ns	0.4252
	Ctrl vs. Emx1-cKO	0	0	0	-88.51 to 88.51	ns	>0.9999
	Nex-cKO vs. Emx1-cKO	46.89	0	46.89	-47.73 to 141.5	ns	0.4728
3	Ctrl vs. Nex-cKO	0	98.1	-98.1	-186.6 to -9.584	*	0.0257
	Ctrl vs. Emx1-cKO	0	0	0	-88.51 to 88.51	ns	>0.9999
	Nex-cKO vs. Emx1-cKO	98.1	0	98.1	3.473 to 192.7	*	0.0402
4	Ctrl vs. Nex-cKO	0	126.2	-126.2	-214.7 to -37.72	**	0.0026
	Ctrl vs. Emx1-cKO	0	0	0	-88.51 to 88.51	ns	>0.9999
	Nex-cKO vs. Emx1-cKO	126.2	0	126.2	31.6 to 220.9	**	0.0053
5	Ctrl vs. Nex-cKO	18.5	111	-92.51	-181 to -3.999	*	0.0382
	Ctrl vs. Emx1-cKO	18.5	13.31	5.196	-83.32 to 93.71	ns	0.9895
	Nex-cKO vs. Emx1-cKO	111	13.31	97.71	3.084 to 192.3	*	0.0412
6	Ctrl vs. Nex-cKO	69.28	128.1	-58.82	-147.3 to 29.69	ns	0.2617
	Ctrl vs. Emx1-cKO	69.28	97.47	-28.19	-116.7 to 60.32	ns	0.7331
	Nex-cKO vs. Emx1-cKO	128.1	97.47	30.63	-63.99 to 125.3	ns	0.7256
7	Ctrl vs. Nex-cKO	107.5	176	-68.56	-300.3 to 163.2	ns	0.765
	Ctrl vs. Emx1-cKO	107.5	152.1	-44.66	-227.9 to 138.6	ns	0.8336
	Nex-cKO vs. Emx1-cKO	176	152.1	23.9	-159.3 to 207.1	ns	0.9491
8	Ctrl vs. Nex-cKO	175.2	237.2	-61.95	-157.9 to 34.02	ns	0.2821
	Ctrl vs. Emx1-cKO	175.2	154.5	20.69	-70.49 to 111.9	ns	0.8541
	Nex-cKO vs. Emx1-cKO	237.2	154.5	82.63	-16.61 to 181.9	ns	0.1235
9	Ctrl vs. Nex-cKO	214.5	138.2	76.34	-12.17 to 164.9	ns	0.1063
	Ctrl vs. Emx1-cKO	214.5	197.7	16.82	-71.69 to 105.3	ns	0.8952
	Nex-cKO vs. Emx1-cKO	138.2	197.7	-59.52	-154.1 to 35.1	ns	0.3005
10	Ctrl vs. Nex-cKO	209.6	115.1	94.49	5.983 to 183	*	0.0333
	Ctrl vs. Emx1-cKO	209.6	132	77.6	-10.91 to 166.1	ns	0.0988
	Nex-cKO vs. Emx1-cKO	115.1	132	-16.89	-111.5 to 77.73	ns	0.9069
11	Ctrl vs. Nex-cKO	232.5	99.13	133.4	44.9 to 221.9	**	0.0013
	Ctrl vs. Emx1-cKO	232.5	116.2	116.4	27.87 to 204.9	**	0.0061
	Nex-cKO vs. Emx1-cKO	99.13	116.2	-17.03	-111.7 to 77.59	ns	0.9055
12	Ctrl vs. Nex-cKO	186.4	127.8	58.65	-34.78 to 152.1	ns	0.302
	Ctrl vs. Emx1-cKO	186.4	26.38	160.1	71.56 to 248.6	****	<0.0001
	Nex-cKO vs. Emx1-cKO	127.8	26.38	101.4	2.179 to 200.7	*	0.0439
13	Ctrl vs. Nex-cKO	94.47	0	94.47	-137.3 to 326.2	ns	0.6019
	Ctrl vs. Emx1-cKO	94.47	13.38	81.09	-95.93 to 258.1	ns	0.527
	Nex-cKO vs. Emx1-cKO	0	13.38	-13.38	-190.4 to 163.6	ns	0.9826

<b>14</b>	<i>Ctrl vs. Nex-cKO</i>	58.1	0	58.1	-33.08 to 149.3	ns	0.2913
	<i>Ctrl vs. Emx1-cKO</i>	58.1	0	58.1	-33.08 to 149.3	ns	0.2913
	<i>Nex-cKO vs. Emx1-cKO</i>	0	0	0	-94.62 to 94.62	ns	>0.9999
<b>15</b>	<i>Ctrl vs. Nex-cKO</i>	0	0	0	-84.82 to 84.82	ns	>0.9999
	<i>Ctrl vs. Emx1-cKO</i>	0	0	0	-88.51 to 88.51	ns	>0.9999
	<i>Nex-cKO vs. Emx1-cKO</i>	0	0	0	-91.18 to 91.18	ns	>0.9999
<b>Figure 5G – Rostral LFP area</b>							
	<b>Hypothesis</b>	<b>Mean 1</b>	<b>Mean 2</b>	<b>Mean diff.</b>	<b>95,00% CI of diff</b>	<b>Summary</b>	<b>Adjusted P.</b>
	<i>Ctrl vs. Nex-cKO</i>	2414	2258	156.4	-570.3 to 883	ns	0.8257
	<i>Ctrl vs. Emx1-cKO</i>	2414	1725	689.2	-37.42 to 1416	ns	0.0637
<b>Figure 5H – Caudal LFP area</b>							
	<b>Hypothesis</b>	<b>Mean 1</b>	<b>Mean 2</b>	<b>Mean diff.</b>	<b>95,00% CI of diff</b>	<b>Summary</b>	<b>Adjusted P.</b>
	<i>Ctrl vs. Nex-cKO</i>	1403	1427	-24.29	-261.8 to 213.2	ns	0.9566
	<i>Ctrl vs. Emx1-cKO</i>	1403	884.1	518.8	281.3 to 756.3	***	0.0001
<b>Figure 5I – Fasciculation Index</b>							
<b>Region</b>	<b>Hypothesis</b>	<b>Mean 1</b>	<b>Mean 2</b>	<b>Mean diff.</b>	<b>95,00% CI of diff</b>	<b>Summary</b>	<b>Adjusted P.</b>
<b>250 μm</b>	<i>Ctrl vs. Nex-cKO</i>	0.6528	0.5493	0.1035	0.01185 to 0.1951	*	0.0216
	<i>Ctrl vs. Emx1-cKO</i>	0.6528	0.5595	0.09326	0.001658 to 0.1849	*	0.0446
<b>500 μm</b>	<i>Ctrl vs. Nex-cKO</i>	0.674	0.5771	0.0969	0.00254 to 0.1913	*	0.0422
	<i>Ctrl vs. Emx1-cKO</i>	0.674	0.5146	0.1594	0.06502 to 0.2537	***	0.0004

832

833 **Summary of statistical analysis and results.** Highlighted in blue, comparisons that produced  
 834 statistically significant P-values. P-values are calculated by 2way ANOVA test (**Figures 4F and 5E-F**), or  
 835 ordinary one-way ANOVA test (**Figures 5G-I**).

836

837

838 **Supplementary Table 5: List of primary and secondary antibodies used in this study.**

Antigen	Provider	Catalog #	Species	Working dilution
GFP	Abcam	Ab13970	Ck	1:500
RFP	Abcam	Ab 124754	Rb	1:500
Ck IgY - AF 488	Thermo Fisher	A11039	Gt	1:500
Rb IgG - AF 555	Thermo Fisher	A21428	Gt	1:500

839



840 **REFERENCES:**

- 841 Alfano, C., Magrinelli, E., Harb, K., Hevner, R. F. and Studer, M. (2014) 'Postmitotic control of  
842 sensory area specification during neocortical development', *Nat Commun*, 5, pp.  
843 5632.
- 844 Alfano, C. and Studer, M. (2012) 'Neocortical arealization: Evolution, mechanisms and open  
845 questions', *Dev Neurobiol*.
- 846 Altman, J. and Bayer, S. A. (1987) 'Development of the precerebellar nuclei in the rat: IV. The  
847 anterior precerebellar extramural migratory stream and the nucleus reticularis  
848 tegmenti pontis and the basal pontine gray', *J Comp Neurol*, 257(4), pp. 529-52.
- 849 Altman J, Bayer SA (1996) Development of the cerebellar system in relation to its evolution,  
850 structure and functions. CRC Press, Boca Raton
- 851 Armentano, M., Chou, S. J., Tomassy, G. S., Leingartner, A., O'Leary, D. D. and Studer, M.  
852 (2007) 'COUP-TFI regulates the balance of cortical patterning between frontal/motor  
853 and sensory areas', *Nat Neurosci*, 10(10), pp. 1277-86.
- 854 Assimacopoulos, S., Kao, T., Issa, N. P. and Grove, E. A. (2012) 'Fibroblast growth factor 8  
855 organizes the neocortical area map and regulates sensory map topography', *J*  
856 *Neurosci*, 32(21), pp. 7191-201.
- 857 Badura, A., Schonewille, M., Voges, K., Galliano, E., Renier, N., Gao, Z., Witter, L., Hoebeek,  
858 F. E., Chedotal, A. and De Zeeuw, C. I. (2013) 'Climbing fiber input shapes reciprocity  
859 of Purkinje cell firing', *Neuron*, 78(4), pp. 700-13.
- 860 Bertacchi, M., Parisot, J. and Studer, M. (2019) 'The pleiotropic transcriptional regulator  
861 COUP-TFI plays multiple roles in neural development and disease', *Brain Res*, 1705,  
862 pp. 75-94.
- 863 Bjaalie, J. G. and Brodal, P. (1989) 'Visual pathways to the cerebellum: segregation in the  
864 pontine nuclei of terminal fields from different visual cortical areas in the cat',  
865 *Neuroscience*, 29(1), pp. 95-107.
- 866 Bjaalie, J. G. and Brodal, P. (1997) 'Cat pontocerebellar network: numerical capacity and  
867 axonal collateral branching of neurones in the pontine nuclei projecting to individual  
868 parafloccular folia', *Neurosci Res*, 27(3), pp. 199-210.
- 869 Bower, J. M. (2011) 'Functional implications of tactile projection patterns to the lateral  
870 hemispheres of the cerebellum of the albino rat: the legacy of Wally Welker', *Ann N*  
871 *Y Acad Sci*, 1225, pp. 130-41.
- 872 Bower, J. M., Beermann, D. H., Gibson, J. M., Shambes, G. M. and Welker, W. (1981)  
873 'Principles of organization of a cerebro-cerebellar circuit. Micromapping the  
874 projections from cerebral (SI) to cerebellar (granule cell layer) tactile areas of rats',  
875 *Brain Behav Evol*, 18(1-2), pp. 1-18.
- 876 Bower, J. M. and Kassel, J. (1990) 'Variability in tactile projection patterns to cerebellar folia  
877 crus IIA of the Norway rat', *J Comp Neurol*, 302(4), pp. 768-78.
- 878 Brodal, P. (1978) 'The corticopontine projection in the rhesus monkey. Origin and principles  
879 of organization', *Brain*, 101(2), pp. 251-83.
- 880 Brodal, P. and Bjaalie, J. G. (1992) 'Organization of the pontine nuclei', *Neurosci Res*, 13(2),  
881 pp. 83-118.
- 882 Buckner, R. L. (2013) 'The cerebellum and cognitive function: 25 years of insight from  
883 anatomy and neuroimaging', *Neuron*, 80(3), pp. 807-15.
- 884 Cadwell, C. R., Bhaduri, A., Mostajo-Radji, M. A., Keefe, M. G. and Nowakowski, T. J. (2019)  
885 'Development and Arealization of the Cerebral Cortex', *Neuron*, 103(6), pp. 980-  
886 1004.

- 887 Cederquist, G. Y., Azim, E., Shnider, S. J., Padmanabhan, H. and Macklis, J. D. (2013) 'Lmo4  
888 establishes rostral motor cortex projection neuron subtype diversity', *J Neurosci*,  
889 33(15), pp. 6321-32.
- 890 Chapin, J. K. and Lin, C. S. (1984) 'Mapping the body representation in the SI cortex of  
891 anesthetized and awake rats', *J Comp Neurol*, 229(2), pp. 199-213.
- 892 D'Elia, K. P. and Dasen, J. S. (2018) 'Topographic Maps: Motor Axons Wait Their Turn', *Curr*  
893 *Biol*, 28(2), pp. R86-R88.
- 894 Del Pino, I., Tocco, C., Magrinelli, E., Marcantoni, A., Ferraguto, C., Tomagra, G., Bertacchi,  
895 M., Alfano, C., Leinekugel, X., Frick, A. and Studer, M. (2020) 'COUP-TFI/Nr2f1  
896 Orchestrates Intrinsic Neuronal Activity during Development of the Somatosensory  
897 Cortex', *Cereb Cortex*, 30(11), pp. 5667-5685.
- 898 Erzurumlu, R. S., Murakami, Y. and Rijli, F. M. (2010) 'Mapping the face in the  
899 somatosensory brainstem', *Nat Rev Neurosci*, 11(4), pp. 252-63.
- 900 Fabri, M. and Burton, H. (1991) 'Ipsilateral cortical connections of primary somatic sensory  
901 cortex in rats', *J Comp Neurol*, 311(3), pp. 405-24.
- 902 Feng, G., Mellor, R. H., Bernstein, M., Keller-Peck, C., Nguyen, Q. T., Wallace, M., Nerbonne,  
903 J. M., Lichtman, J. W. and Sanes, J. R. (2000) 'Imaging neuronal subsets in transgenic  
904 mice expressing multiple spectral variants of GFP', *Neuron*, 28(1), pp. 41-51.
- 905 Flore, G., Di Ruberto, G., Parisot, J., Sannino, S., Russo, F., Illingworth, E. A., Studer, M. and  
906 De Leonibus, E. (2017) 'Gradient COUP-TFI Expression Is Required for Functional  
907 Organization of the Hippocampal Septo-Temporal Longitudinal Axis', *Cereb Cortex*,  
908 27(2), pp. 1629-1643.
- 909 Fritsch, B., Elliott, K. L. and Pavlinkova, G. (2019) 'Primary sensory map formations reflect  
910 unique needs and molecular cues specific to each sensory system', *F1000Res*, 8.
- 911 Goebbels, S., Bormuth, I., Bode, U., Hermanson, O., Schwab, M. H. and Nave, K. A. (2006)  
912 'Genetic targeting of principal neurons in neocortex and hippocampus of NEX-Cre  
913 mice', *Genesis*, 44(12), pp. 611-21.
- 914 Greig, L. C., Woodworth, M. B., Galazo, M. J., Padmanabhan, H. and Macklis, J. D. (2013)  
915 'Molecular logic of neocortical projection neuron specification, development and  
916 diversity', *Nat Rev Neurosci*, 14(11), pp. 755-69.
- 917 Harb, K., Magrinelli, E., Nicolas, C. S., Lukianets, N., Frangeul, L., Pietri, M., Sun, T., Sandoz,  
918 G., Grammont, F., Jabaudon, D., Studer, M. and Alfano, C. (2016) 'Area-specific  
919 development of distinct projection neuron subclasses is regulated by postnatal  
920 epigenetic modifications', *Elife*, 5.
- 921 Heffner, C. D., Lumsden, A. G. and O'Leary, D. D. (1990) 'Target control of collateral  
922 extension and directional axon growth in the mammalian brain', *Science*, 247(4939),  
923 pp. 217-20.
- 924 Henschke, J. U. and Pakan, J. M. (2020) 'Disynaptic cerebocerebellar pathways originating  
925 from multiple functionally distinct cortical areas', *Elife*, 9.
- 926 Inoue, K., Terashima, T. and Inoue, Y. (1991) 'Postnatal development of the pontine  
927 projections from the visual cortex of the mouse', *Okajimas Folia Anat Jpn*, 67(6), pp.  
928 479-92.
- 929 Leergaard, T. B. (2003) 'Clustered and laminar topographic patterns in rat cerebro-pontine  
930 pathways', *Anat Embryol (Berl)*, 206(3), pp. 149-62.
- 931 Leergaard, T. B., Alloway, K. D., Mutic, J. J. and Bjaalie, J. G. (2000a) 'Three-dimensional  
932 topography of corticopontine projections from rat barrel cortex: correlations with  
933 corticostriatal organization', *J Neurosci*, 20(22), pp. 8474-84.

- 934 Leergaard, T. B., Alloway, K. D., Pham, T. A., Bolstad, I., Hoffer, Z. S., Pettersen, C. and  
935 Bjaalie, J. G. (2004) 'Three-dimensional topography of corticopontine projections  
936 from rat sensorimotor cortex: comparisons with corticostriatal projections reveal  
937 diverse integrative organization', *J Comp Neurol*, 478(3), pp. 306-22.
- 938 Leergaard, T. B. and Bjaalie, J. G. (1995) 'Semi-automatic data acquisition for quantitative  
939 neuroanatomy. MicroTrace--computer programme for recording of the spatial  
940 distribution of neuronal populations', *Neurosci Res*, 22(2), pp. 231-43.
- 941 Leergaard, T. B. and Bjaalie, J. G. (2007) 'Topography of the complete corticopontine  
942 projection: from experiments to principal Maps', *Front Neurosci*, 1(1), pp. 211-23.
- 943 Leergaard, T. B., Lakke, E. A. and Bjaalie, J. G. (1995) 'Topographical organization in the early  
944 postnatal corticopontine projection: a carbocyanine dye and 3-D computer  
945 reconstruction study in the rat', *J Comp Neurol*, 361(1), pp. 77-94.
- 946 Leergaard, T. B., Lillehaug, S., De Schutter, E., Bower, J. M. and Bjaalie, J. G. (2006)  
947 'Topographical organization of pathways from somatosensory cortex through the  
948 pontine nuclei to tactile regions of the rat cerebellar hemispheres', *Eur J Neurosci*,  
949 24(10), pp. 2801-12.
- 950 Leergaard, T. B., Lyngstad, K. A., Thompson, J. H., Taeymans, S., Vos, B. P., De Schutter, E.,  
951 Bower, J. M. and Bjaalie, J. G. (2000b) 'Rat somatosensory cerebropontocerebellar  
952 pathways: spatial relationships of the somatotopic map of the primary  
953 somatosensory cortex are preserved in a three-dimensional clustered pontine map',  
954 *J Comp Neurol*, 422(2), pp. 246-66.
- 955 Lemon, R. N. (2008) 'Descending pathways in motor control', *Annu Rev Neurosci*, 31, pp.  
956 195-218.
- 957 Lillehaug, S., Oyan, D., Leergaard, T. B. and Bjaalie, J. G. (2002) 'Comparison of semi-  
958 automatic and automatic data acquisition methods for studying three-dimensional  
959 distributions of large neuronal populations and axonal plexuses', *Network*, 13(3), pp.  
960 343-56.
- 961 Liu, Q., Dwyer, N. D. and O'Leary, D. D. (2000) 'Differential expression of COUP-TFI, CHL1,  
962 and two novel genes in developing neocortex identified by differential display PCR', *J  
963 Neurosci*, 20(20), pp. 7682-90.
- 964 Maheshwari, U., Kraus, D., Vilain, N., Holwerda, S. J. B., Cankovic, V., Maiorano, N. A.,  
965 Kohler, H., Satoh, D., Sigrist, M., Arber, S., Kratochwil, C. F., Di Meglio, T., Ducret, S.  
966 and Rijli, F. M. (2020) 'Postmitotic Hoxa5 Expression Specifies Pontine Neuron  
967 Positional Identity and Input Connectivity of Cortical Afferent Subsets', *Cell Rep*,  
968 31(11), pp. 107767.
- 969 McLaughlin, T. and O'Leary, D. D. (2005) 'Molecular gradients and development of  
970 retinotopic maps', *Annu Rev Neurosci*, 28, pp. 327-55.
- 971 Mercurio, S., Serra, L., Motta, A., Gesuita, L., Sanchez-Arrones, L., Inverardi, F., Foglio, B.,  
972 Barone, C., Kaimakis, P., Martynoga, B., Ottolenghi, S., Studer, M., Guillemot, F.,  
973 Frassoni, C., Bovolenta, P. and Nicolis, S. K. (2019) 'Sox2 Acts in Thalamic Neurons to  
974 Control the Development of Retina-Thalamus-Cortex Connectivity', *iScience*, 15, pp.  
975 257-273.
- 976 Mihailoff, G. A., Lee, H., Watt, C. B. and Yates, R. (1985) 'Projections to the basilar pontine  
977 nuclei from face sensory and motor regions of the cerebral cortex in the rat', *J Comp  
978 Neurol*, 237(2), pp. 251-63.

- 979 Mottolese, C., Richard, N., Harquel, S., Szathmari, A., Sirigu, A. and Desmurget, M. (2013)  
980 'Mapping motor representations in the human cerebellum', *Brain*, 136(Pt 1), pp. 330-  
981 42.
- 982 Nitschke, M. F., Kleinschmidt, A., Wessel, K. and Frahm, J. (1996) 'Somatotopic motor  
983 representation in the human anterior cerebellum. A high-resolution functional MRI  
984 study', *Brain*, 119 ( Pt 3), pp. 1023-9.
- 985 O'Leary, D. D. and Nakagawa, Y. (2002) 'Patterning centers, regulatory genes and extrinsic  
986 mechanisms controlling arealization of the neocortex', *Curr Opin Neurobiol*, 12(1),  
987 pp. 14-25.
- 988 O'Leary, D. D. and Sahara, S. (2008) 'Genetic regulation of arealization of the neocortex',  
989 *Curr Opin Neurobiol*, 18(1), pp. 90-100.
- 990 O'Leary, D. D. and Terashima, T. (1988) 'Cortical axons branch to multiple subcortical targets  
991 by interstitial axon budding: implications for target recognition and "waiting  
992 periods"', *Neuron*, 1(10), pp. 901-10.
- 993 Peterburs, J. and Desmond, J. E. (2016) 'The role of the human cerebellum in performance  
994 monitoring', *Curr Opin Neurobiol*, 40, pp. 38-44.
- 995 Petersen, S. C., Watson, J. D., Richmond, J. E., Sarov, M., Walthall, W. W. and Miller, D. M.,  
996 3rd (2011) 'A transcriptional program promotes remodeling of GABAergic synapses  
997 in *Caenorhabditis elegans*', *J Neurosci*, 31(43), pp. 15362-75.
- 998 Polleux, F., Dehay, C. and Kennedy, H. (1997) 'The timetable of laminar neurogenesis  
999 contributes to the specification of cortical areas in mouse isocortex', *J Comp Neurol*,  
1000 385(1), pp. 95-116.
- 1001 Porrero, C., Rubio-Garrido, P., Avendano, C. and Clasca, F. (2010) 'Mapping of fluorescent  
1002 protein-expressing neurons and axon pathways in adult and developing Thy1-eYFP-H  
1003 transgenic mice', *Brain Res*, 1345, pp. 59-72.
- 1004 Pourchet, O., Morel, M. P., Welniarz, Q., Sarrazin, N., Marti, F., Heck, N., Gallea, C.,  
1005 Doulazmi, M., Roig Puiggros, S., Moreno-Bravo, J. A., Vidailhet, M., Trembleau, A.,  
1006 Faure, P., Chedotal, A., Roze, E. and Dusart, I. (2021) 'Loss of floor plate Netrin-1  
1007 impairs midline crossing of corticospinal axons and leads to mirror movements', *Cell*  
1008 *Rep*, 34(3), pp. 108654.
- 1009 Proville, R. D., Spolidoro, M., Guyon, N., Dugue, G. P., Selimi, F., Isope, P., Popa, D. and Lena,  
1010 C. (2014) 'Cerebellum involvement in cortical sensorimotor circuits for the control of  
1011 voluntary movements', *Nat Neurosci*, 17(9), pp. 1233-9.
- 1012 Puchades, M. A., Csucs, G., Ledergerber, D., Leergaard, T. B. and Bjaalie, J. G. (2019) 'Spatial  
1013 registration of serial microscopic brain images to three-dimensional reference  
1014 atlases with the QuickNII tool', *PLoS One*, 14(5), pp. e0216796.
- 1015 Schindelin, J., Rueden, C. T., Hiner, M. C. and Eliceiri, K. W. (2015) 'The ImageJ ecosystem: An  
1016 open platform for biomedical image analysis', *Mol Reprod Dev*, 82(7-8), pp. 518-29.
- 1017 Schmahmann, J. D. and Pandya, D. N. (1997) 'Anatomic organization of the basilar pontine  
1018 projections from prefrontal cortices in rhesus monkey', *J Neurosci*, 17(1), pp. 438-58.
- 1019 Shambes, G. M., Gibson, J. M. and Welker, W. (1978) 'Fractured somatotopy in granule cell  
1020 tactile areas of rat cerebellar hemispheres revealed by micromapping', *Brain Behav*  
1021 *Evol*, 15(2), pp. 94-140.
- 1022 Shepherd, G. M. (2009) 'Intracortical cartography in an agranular area', *Front Neurosci*, 3(3),  
1023 pp. 337-43.
- 1024 Smart, I. H. (1984) 'Histogenesis of the mesocortical area of the mouse telencephalon', *J*  
1025 *Anat*, 138 ( Pt 3), pp. 537-52.

- 1026 Stoodley, C. J. and Schmahmann, J. D. (2010) 'Evidence for topographic organization in the  
1027 cerebellum of motor control versus cognitive and affective processing', *Cortex*, 46(7),  
1028 pp. 831-44.
- 1029 Tomasch, J. (1968) 'The overall information carrying capacity of the major afferent and  
1030 efferent cerebellar cell and fiber systems', *Confin Neurol*, 30(5), pp. 359-67.
- 1031 Tomasch, J. (1969) '[The renal pelvis of the dromedary]', *Z Anat Entwicklungsgesch*, 128(3),  
1032 pp. 235-42.
- 1033 Tomassy, G. S., De Leonibus, E., Jabaudon, D., Lodato, S., Alfano, C., Mele, A., Macklis, J. D.  
1034 and Studer, M. (2010) 'Area-specific temporal control of corticospinal motor neuron  
1035 differentiation by COUP-TFI', *Proc Natl Acad Sci U S A*, 107(8), pp. 3576-81.
- 1036 Wang, Q., Ding, S. L., Li, Y., Royall, J., Feng, D., Lesnar, P., Graddis, N., Naeemi, M., Facer, B.,  
1037 Ho, A., Dolbeare, T., Blanchard, B., Dee, N., Wakeman, W., Hirokawa, K. E., Szafer, A.,  
1038 Sunkin, S. M., Oh, S. W., Bernard, A., Phillips, J. W., Hawrylycz, M., Koch, C., Zeng, H.,  
1039 Harris, J. A. and Ng, L. (2020) 'The Allen Mouse Brain Common Coordinate  
1040 Framework: A 3D Reference Atlas', *Cell*, 181(4), pp. 936-953 e20.
- 1041 Welker, C. (1971) 'Microelectrode delineation of fine grain somatotopic organization of  
1042 (Sml) cerebral neocortex in albino rat', *Brain Res*, 26(2), pp. 259-75.
- 1043 Woolsey, T. A. and Van der Loos, H. (1970) 'The structural organization of layer IV in the  
1044 somatosensory region (SI) of mouse cerebral cortex. The description of a cortical  
1045 field composed of discrete cytoarchitectonic units', *Brain Res*, 17(2), pp. 205-42.
- 1046 Zhou, C., Tsai, S. Y. and Tsai, M. J. (2001) 'COUP-TFI: an intrinsic factor for early  
1047 regionalization of the neocortex', *Genes Dev*, 15(16), pp. 2054-9.
- 1048 Zhou, H. M. and Walthall, W. W. (1998) 'UNC-55, an orphan nuclear hormone receptor,  
1049 orchestrates synaptic specificity among two classes of motor neurons in  
1050 *Caenorhabditis elegans*', *J Neurosci*, 18(24), pp. 10438-44.
- 1051